



IMPLEMENTING MULTI-SCALE AGRICULTURAL INDICATORS EXPLOITING SENTINELS

**VEGETATION FIELD DATA AND PRODUCTION OF
GROUND-BASED MAPS:**

**“LAS TIESAS - BARRAX SITE, ALBACETE, SPAIN”
27TH MAY AND 22ND JULY, 2015**

ISSUE I1.00

EC Proposal Reference N° FP7-311766

Actual submission date : September 2015

Start date of project: 01.11.2012

Duration : 40 months

Name of lead partner for this deliverable: EOLAB



Book Captain: Consuelo Latorre (EOLAB)

Contributing Authors: Fernando Camacho, María del Carmen Piñó (EOLAB)

Fernando de la Cruz (ITAP)

Project co-funded by the European Commission within the Seventh Framework Program (2007-2013)		
Dissemination Level		
PU	Public	X
PP	Restricted to other programme participants (including the Commission Services)	
RE	Restricted to a group specified by the consortium (including the Commission Services)	
CO	Confidential, only for members of the consortium (including the Commission Services)	

DOCUMENT RELEASE SHEET

Book Captain:	C. Latorre	Date: 21.09.2015	Sign. 
Approval:	R. Lacaze	Date: 14.12.2015	Sign. 
Endorsement:	I. Marin-Moreno	Date:	Sign.
Distribution:			

CHANGE RECORD

Issue/Revision	Date	Page(s)	Description of Change	Release
	21.09.2015	All	First Issue	I1.00

TABLE OF CONTENTS

1.	<i>Background of the Document</i>	11
1.1.	Executive Summary	11
1.2.	Portfolio	11
1.3.	Scope and Objectives	12
1.4.	Content of the Document	12
2.	<i>Introduction</i>	13
3.	<i>Study area</i>	16
3.1.	Location	16
3.2.	Description of The Test Site	17
4.	<i>Ground measurements</i>	19
4.1.	Material and Methods	19
4.1.1	Digital Hemispheric Photographs (DHP)	19
4.1.2	AccuPARLP80-Ceptometer	22
4.1.3	LI-COR LAI-2200C plant canopy analyser	23
4.2.	Spatial Sampling Scheme	24
4.3.	Ground data	25
4.3.1.	Data processing	25
4.3.2.	Content of the Ground Dataset	30
5.	<i>Evaluation of the sampling</i>	35
5.1.	Principles	35
5.2.	Evaluation Based On NDVI Values	35
5.3.	Evaluation Based On Convex Hull: Product Quality Flag	36
6.	<i>Production of ground-based maps</i>	38
6.1.	Imagery	38
6.2.	The Transfer Function	38
6.2.1.	The regression method	39
6.2.2.	Band combination	39
6.2.3.	The selected Transfer Function	40
6.3.	The High Resolution Ground Based Maps	43
6.3.1.	Mean Values	47

7.	<i>Conclusions</i>	<i>49</i>
8.	<i>Acknowledgements.....</i>	<i>50</i>
9.	<i>References</i>	<i>51</i>
10.	<i>Annex I: Description of ESUs.....</i>	<i>53</i>

LIST OF FIGURES

Figure 1: Team involved in the field campaign of Las Tiesas site in Barrax, Spain (2015). Top -Left: Measurements with LAI2200C over a papaver somniferum field, operator Fernando Camacho. Top- Right: Measurements with ceptometer LP80 over a sunflower field, operator María del Carmen Piñó. Bottom: field of corn where the PASTIS-PAR devices were installed on 27 th May (left) and 22 nd July (right), operator Consuelo Latorre.....	14
Figure 2: Location of Las Tiesas site in Barrax, Spain.	16
Figure 3: False color composition (RGB – SWIR-NIR-RED) of TOC Reflectance Landsat-8 images over the study area 20 km ² . (Barrax, 07 th June (left) and 16 th July (right), 2015). The red square outlines the 5 km ² area of interest.	17
Figure 4: Land use map (winter and spring seasons) of Las Tiesas - Barrax (Spain).	18
Figure 5: Pictures taken during the first field campaign (May, 2015) in Las Tiesas - Barrax (Spain).	18
Figure 6: AccuPAR LP80-Ceptometer	22
Figure 7: LAI-2200C device.	23
Figure 8: LAI-2200 optical sensor with 5 zenith angles	24
Figure 9: Distribution of the Elementary Sampling Units (ESU) over the study area of Las Tiesas - Barrax site. Left: First field campaign (27 th May 2015). Right: Second field campaign (22 nd July 2015). DHP, LAI2200C and LP80 sampling (orange and blue), visual inspection ESUs (white) and ground control points (red).	24
Figure 10: Distribution of vegetation types sampled during the field campaigns. Las Tiesas – Barrax site (Spain) 2015. Left: First field campaign (27 th May). Right: Second field campaign (22 nd July).	25
Figure 11: Digital Hemispherical Photographs acquired in Las Tiesas - Barrax site (Spain) during the field campaigns in 2015. Top: First field campaign (27 th May). Bottom: Second field campaign (22 nd July).	26
Figure 12: Results of the CAN-EYE processing carried out on a Garlic crop ESU (Garlic G1 - ESU 14) during the first field campaign (27 th May, 2015). (a) DHP images. (b) Classified images. (c) Average gap fraction and (d) the clumping factor versus view zenith angle.	26
Figure 13: Inter-comparison of the calculated biophysical variables LAI (left side) and LAI _{eff} (right side) over the ESUs with different methods: CEV5.1, CEV6.1 and Miller's formula. Las Tiesas site – Barrax (Spain) during the campaign of 27 th May, 2015.	27
Figure 14: Inter-comparison of the calculated biophysical variables LAI (left side) and LAI _{eff} (right side) over the ESUs with different methods: CEV5.1, CEV6.1 and Miller's formula. Las Tiesas site – Barrax (Spain) during the campaign of 22 nd July, 2015.	27
Figure 15: Intercomparison of the measured biophysical variables over the ESUs. Effective LAI and LAI versus FAPAR, Las Tiesas site – Barrax (Spain). Left side: First field campaign (27 th May). Right side: Second field campaign (22 nd July).	28
Figure 16: Intercomparison of the measured biophysical variables over the ESUs. FAPAR versus FCOVER, Las Tiesas site – Barrax (Spain). Left side: First field campaign (27 th May). Right side: Second field campaign (22 nd July).	28
Figure 17: Results of the clumping processing by CAN-EYE carried out on two ESUs during the first field campaign (27 th May 2015), Barrax. Left side: ESU 21, wheat field. Right side: ESU 10, papaver somniferum field.	29
Figure 18: LAI _{eff} measurements acquired in Las Tiesas site – Barrax, during the field campaigns, 2015. Top: first campaign, 26 th – 28 th May. Bottom: second campaign, 22 nd July.	31
Figure 19: As in Figure 18 for LAI.....	32

Figure 20: As in Figure 18 for FAPAR 10:00 SLT and daily integrated FAPAR.....	32
Figure 21: As in Figure 18 for FCOVER.....	33
Figure 22: Distribution of the measured biophysical variables over the ESUs, Las Tiasas site – Barrax, during the first campaign on 27 th May, 2015.	33
Figure 23: Distribution of the measured biophysical variables over the ESUs, Las Tiasas site – Barrax, during the second campaign on 22 nd July, 2015.	34
Figure 24: Comparison of NDVI TOC distribution between ESUs (brown dots) and over the whole image (blue line). Las Tiasas – Barrax (2015). Left: First field campaign (27 th May). Right: Second field campaign (22 nd July).	36
Figure 25: Convex Hull test over 20x20 km ² (left side) and 5x5 km ² (right side) areas: clear and dark blue correspond to the pixels belonging to the ‘strict’ and ‘large’ convex hulls. Red corresponds to the pixels for which the transfer function is extrapolating, Las Tiasas – Barrax, 2015. Top: First field campaign (27 th May). Bottom: Second field campaign (22 nd July).	37
Figure 26: Test of multiple regression (TF) applied on different band combinations. Band combinations are given in abscissa (1=G, 2=RED, 3=NIR and 4=SWIR). The weighted root mean square error (RMSE) is presented in red along with the cross-validation RMSE in green. The numbers indicate the number of data used for the robust regression with a weight lower than 0.7 that could be considered as outliers. Barrax, first field campaign on 27 th May 2015.	39
Figure 27: As in Figure 26 for the second campaign on 22 nd July, 2015.	40
Figure 28: LAIeff, LAI, FAPAR and FCOVER results for regression on NDVI. Full dots: Weight>0.7. Empty dots: 0<Weight<0.7. Crosses: Weight=0. Las Tiasas- Barrax, first field campaign 2015 on 27 th May, 2015.	42
Figure 29: As Figure 28 for the second field campaign on 22 nd July, 2015.	43
Figure 30: Ground-based LAIeff maps (20x20 km ²) retrieved on Las Tiasas site – Barrax (Spain) 2015. Left: First field campaign (27 th May). Right: Second field campaign (22 nd July).....	44
Figure 31: Ground-based LAI maps (20x20 km ²) retrieved on Las Tiasas site – Barrax (Spain) 2015. Left: First field campaign (27 th May). Right: Second field campaign (22 nd July).....	44
Figure 32: Ground-based of Instantaneous FAPAR at 10:00 SLT maps (20x20 km ²) retrieved on Las Tiasas site – Barrax (Spain) 2015. Left: First field campaign (27 th May). Right: Second field campaign (22 nd July).	45
Figure 33: Ground-based FCOVER map (20x20 km ²) retrieved on Las Tiasas site – Barrax (Spain) 2015. Left: First field campaign (27 th May). Right: Second field campaign (22 nd July).....	45
Figure 34: Ground-based maps (5x5 km ²) retrieved on the Las Tiasas - Barrax site (Spain). First field campaign on 27 th May, 2015.	46
Figure 35: Ground-based maps (5x5 km ²) retrieved on the Las Tiasas - Barrax site (Spain). Second field campaign on 22 nd July, 2015.	46
Figure 36: Scatter plots to LAI vs FAPAR and FAPAR vs FCOVER for the two campaigns over Las Tiasas site – Barrax (Spain) 2015. Left: First field campaign (27 th May). Right: Second field campaign (22 nd July).	47

LIST OF TABLES

<i>Table 1: Coordinates and altitude of the test site (centre).....</i>	<i>16</i>
<i>Table 2: The Header used to describe ESUs with the ground measurements.</i>	<i>30</i>
<i>Table 3: Percentages of Convex hull results over the study areas (20x20 km² and 5x5 km²) in Barrax, 2015. Convex hull values: 0= extrapolation of TF, 1= strict convex hull and 2= large convex hull.</i>	<i>37</i>
<i>Table 4: Acquisition geometry of Landsat-8 data used for retrieving high resolution maps.</i>	<i>38</i>
<i>Table 5: Transfer function applied to the whole site for LA_{leff}, LAI, instantaneous FAPAR at 10:00 SLT and FCOVER. RW for weighted RMSE, and RC for cross-validation RMSE. NDVI_∞ corresponds to NDVI value for fully developed canopies, and NDVI_s to NDVI value for bare soil areas.....</i>	<i>41</i>
<i>Table 6: Mean values and standard deviation (STD) of the HR biophysical maps for the selected 3 x 3 km² areas at Las Tiesas site – Barrax (Spain) 2015.</i>	<i>48</i>
<i>Table 7: Content of the dataset.....</i>	<i>48</i>

LIST OF ACRONYMS

CEOS	Committee on Earth Observation Satellite
CEOS LPV	Land Product Validation Subgroup
DG AGRI	Directorate General for Agriculture and Rural Development
DG RELEX	Directorate General for External Relations (European Commission)
DHP	Digital Hemispheric Photographs
ECV	Essential Climate Variables
EUROSTATS	Directorate General of the European Commission
ESU	Elementary Sampling Unit
FAPAR	Fraction of Absorbed Photo-synthetically Active Radiation
FAO	Food and Agriculture Organization
FCOVER	Fraction of Vegetation Cover
GCOS	Global Climate Observing System
GEO-GLAM	Global Agricultural Geo- Monitoring Initiative
GIO-GL	GMES Initial Operations - Global Land (GMES)
GCOS	Global Climate Observing System
GMES	Global Monitoring for Environment and Security
GPS	Global Positioning System
IMAGINES	Implementing Multi-scale Agricultural Indicators Exploiting Sentinels
ITAP	<i>Instituto Técnico Agronómico Provincial – Diputación de Albacete.</i>
JECAM	Joint Experiment for Crop Assessment and Monitoring
LAI	Leaf Area Index
LDAS	Land Data Assimilation System
LUT	Look-up-table techniques
PAI	Plant Area Index
PASTIS –PAR	PAI Autonomous System from Transmittance Sensors
PROBA-V	Project for On-Board Autonomy satellite, the V standing for vegetation.
RMSE	Root Mean Square Error
SPOT /VGT	Satellite Pour l'Observation de la Terre / VEGETATION
SCI	GMES Services Coordinated Interface
SLT	Solar Local Time
TOC	Top of Canopy Reflectance
USGS	U.S. Geological Survey Science organization
UTM	Universal Transverse Mercator coordinates system
VALERI	Validation of Land European Remote sensing Instruments
WGCV	Working Group on Calibration and Validation (CEOS)

1. BACKGROUND OF THE DOCUMENT

1.1. EXECUTIVE SUMMARY

The Copernicus Land Service has been built in the framework of the FP7 geoland2 project, which has set up pre-operational infrastructures. ImagineS intends to ensure the continuity of the innovation and development activities of geoland2 to support the operations of the global land component of the GMES Initial Operation (GIO) phase. In particular, the use of the future Sentinel data in an operational context will be prepared. Moreover, IMAGINES will favor the emergence of new downstream activities dedicated to the monitoring of crop and fodder production.

The main objectives of ImagineS are to (i) improve the retrieval of basic biophysical variables, mainly LAI, FAPAR and the surface albedo, identified as Terrestrial Essential Climate Variables, by merging the information coming from different sensors (PROBA-V and Landsat-8) in view to prepare the use of Sentinel missions data; (ii) develop qualified software able to process multi-sensor data at the global scale on a fully automatic basis; (iii) complement and contribute to the existing or future agricultural services by providing new data streams relying upon an original method to assess the above-ground biomass, based on the assimilation of satellite products in a Land Data Assimilation System (LDAS) in order to monitor the crop/fodder biomass production together with the carbon and water fluxes; (iv) demonstrate the added value of this contribution for a community of users acting at global, European, national, and regional scales.

Further, ImagineS serves the growing needs of international (e.g. FAO and NGOs), European (e.g. DG AGRI, EUROSTATS, DG RELEX), and national users (e.g. national services in agro-meteorology, ministries, group of producers, traders) on accurate and reliable information for the implementation of the EU Common Agricultural Policy, of the food security policy, for early warning systems, and trading issues. ImagineS will also contribute to the Global Agricultural Geo-Monitoring Initiative (GEO-GLAM) by its original agriculture service which can monitor crop and fodder production together with the carbon and water fluxes and can provide drought indicators, and through links with JECAM (Joint Experiment for Crop Assessment and Monitoring).

1.2. PORTFOLIO

The ImagineS portfolio contains global and regional biophysical variables derived from multi-sensor satellite data, at different spatial resolutions, together with agricultural indicators, including the above-ground biomass, the carbon and water fluxes, and drought indices resulting from the assimilation of the biophysical variables in the Land Data Assimilation System (LDAS).

The production in Near Real Time of the 333m resolution products, at a frequency of 10 days, using PROBA-V data is carried out in the Copernicus Global Land Service.

The demonstration of high resolution (30m) products derived from Landsat-8 is done over demonstration sites of cropland and grassland in contrasting climatic and environmental conditions.

1.3. SCOPE AND OBJECTIVES

The main objective of this document is to describe the field campaign and ground data collected at Las Tiesas site in Barrax, Spain, and the up-scaling of the ground data to produce ground-based high resolution maps of the following biophysical variables:

- Leaf Area Index (LAI), defined as half of the total developed area of leaves per unit ground surface area (m^2/m^2). We focused on two different LAI quantities (for green elements):
 - The effective LAI (LAI_{eff}) derived from the description of the gap fraction as a function of the view zenith angle. In addition, effective LAI measures derived at 57.5° are also provided in the ground database.
 - The actual LAI (LAI) estimate corrected from the clumping index.
- Fraction of green vegetation cover (FCover), defined as the proportion of soil covered by vegetation, derived from the gap fraction between 0 and 10° of view zenith angle.
- Fraction of Absorbed Photosynthetically Active Radiation (FAPAR), which is the fraction of the photosynthetically active radiation (PAR) absorbed by a vegetation canopy. We are also focused on green elements. PAR is the solar radiation reaching the canopy in the $0.4\text{--}0.7\ \mu\text{m}$ wavelength region. We focused on the instantaneous ‘black-sky’ FAPAR at 10:00h Solar Local Time (SLT), which is the FAPAR under direct illumination conditions at a given solar position. In addition, two other quantities are provided: daily integrated FAPAR computed as the black-sky FAPAR integrated over the day and the ‘white-sky’ FAPAR, which is the FAPAR under diffuse illumination conditions.

1.4. CONTENT OF THE DOCUMENT

This document is structured as follows:

- Chapter 2 provides an introduction to the field experiment.
- Chapter 3 provides the location and description of the site.
- Chapter 4 describes the ground measurements, including material and methods, sampling and data processing.
- Chapter 5 provides an evaluation of the sampling.
- Chapter 6 describes the production of high resolution ground-based maps, and the selected “mean” values for validation.

2. INTRODUCTION

Validation of remote sensing products is mandatory to guaranty that the satellite products meets the user's requirements. Protocols for validation of global LAI products are already developed in the context of Land Product Validation (LPV) group of the Committee on Earth Observation Satellite (CEOS) for the validation of satellite-derived land products (Fernandes et al., 2014), and recently applied to Copernicus global land products based on SPOT/VTG observations (Camacho et al., 2013). This generic approach is made of 2 major components:

- The indirect validation: including inter-comparison between products as well as evaluation of their temporal and spatial consistency
- The direct validation: comparing satellite products to ground measurements of the corresponding biophysical variables. In the case of low and medium resolution sensors, the main difficulty relies on scaling local ground measurements to the extent corresponding to pixels size. However, the direct validation is limited by the small number of sites, for that reason a main objective of ImagineS is the collection of ground truth data in demonstration sites.

The content of this document is compliant with existing validation guidelines (for direct validation) as proposed by the CEOS LPV group (Morissette et al., 2006); the VALERI project (<http://w3.avignon.inra.fr/valeri/>) and ESA campaigns (Baret and Fernandes, 2012). It therefore follows the general strategy based on a bottom up approach: it starts from the scale of the individual measurements that are aggregated over an elementary sampling unit (ESU) corresponding to a support area consistent with that of the high resolution imagery used for the up-scaling of ground data. Several ESUs are sampled over the site. Radiometric values over a decametric image are also extracted over the ESUs. This will be later used to develop empirical transfer functions for up-scaling the ESU ground measurements (e.g. Martínez et al., 2009). Finally, the high resolution ground based map will be compared with the medium resolution satellite product at the spatial support of the product.

One of the demonstration sites of ImagineS is located in the experimental farm of Las Tiesas in Barrax (Albacete, Spain), where a large number of ESA cal/val campaigns were conducted (e.g. Berguer et al., 2001) due to its favorable conditions. Furthermore, this area is a pilot area for downstream applications on irrigation and farming advisory systems from earth observation data (Calera et al., 2005). In the framework of ImagineS a field experiment was conducted during the year 2014 in collaboration with ITAP (*Instituto Técnico Agronómico Provincial*) for the spatial and temporal characterization of the vegetation properties (ImagineS report, Latorre et al., 2015).

During 2015, two main activities were conducted: (1) Two field campaigns on 27th May and 22nd July, 2015 for the spatial characterization of vegetation variables in the study area, conducted by EOLAB, and (2) set-up of PASTIS-PAR (PAI Autonomous System from Transmittance Sensors) systems for the continuous monitoring of FAPAR and Plant Area

Index (PAI). The PASTIS-PAR sensors developed by INRA were installed from May to September.

This report describes the field activities during the two campaigns carried out in 2015. The PASTIS-PAR data were recorded from May to September, and these data will be reported separately at the end of the project.

Field Campaigns:

- **First campaign: 26th – 28th of May, 2015**
- **Second campaign: 22nd of July, 2015**



Figure 1: Team involved in the field campaign of Las Tiesas site in Barrax, Spain (2015). Top -Left: Measurements with LAI2200C over a papaver somniferum field, operator Fernando Camacho. Top- Right: Measurements with ceptometer LP80 over a sunflower field, operator María del Carmen Piñó. Bottom: field of corn where the PASTIS-PAR devices were installed on 27th May (left) and 22nd July (right), operator Consuelo Latorre.

Contact:

EOLAB: Fernando Camacho (fernando.camacho@eolab.es)

ITAP: Fernando De la Cruz (fct.itap@dipualba.es)

Teams involved in field collection (Figure 1):

ITAP: F. De la Cruz

EOLAB: F. Camacho, C. Latorre, M.C. Piñó

3. STUDY AREA

3.1. LOCATION

The study area is located in the experimental farm of “*Las Tiesas*” in Barrax (Albacete, Spain), managed by ITAP (Figure 2 a, b). Barrax test site is situated within La Mancha, a plateau 700 m above sea level (Table 1). The test site is located in the west of Albacete province, around 20 km far away from the capital town.

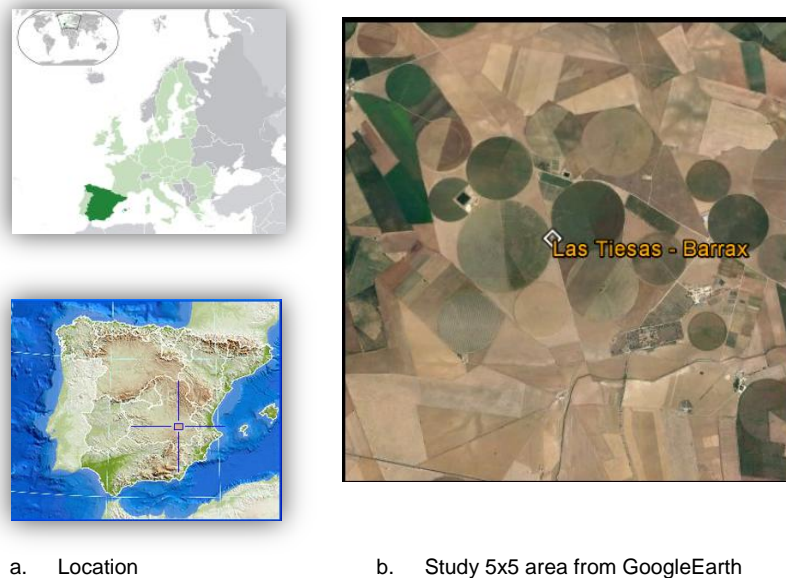


Figure 2: Location of Las Tiesas site in Barrax, Spain.

Table 1: Coordinates and altitude of the test site (centre).

Site Center	
Geographic Lat/lon, WGS-84 (degrees)	Latitude = 39.054371 N Longitude = 2.100677 W
Altitude	700 m

Figure 3 shows the false composition Red Green Blue (RGB) over a Top Of Canopy (TOC) Reflectance Landsat-8 images used for up-scaling the ground dataset. The variations of crop status are readily observed.

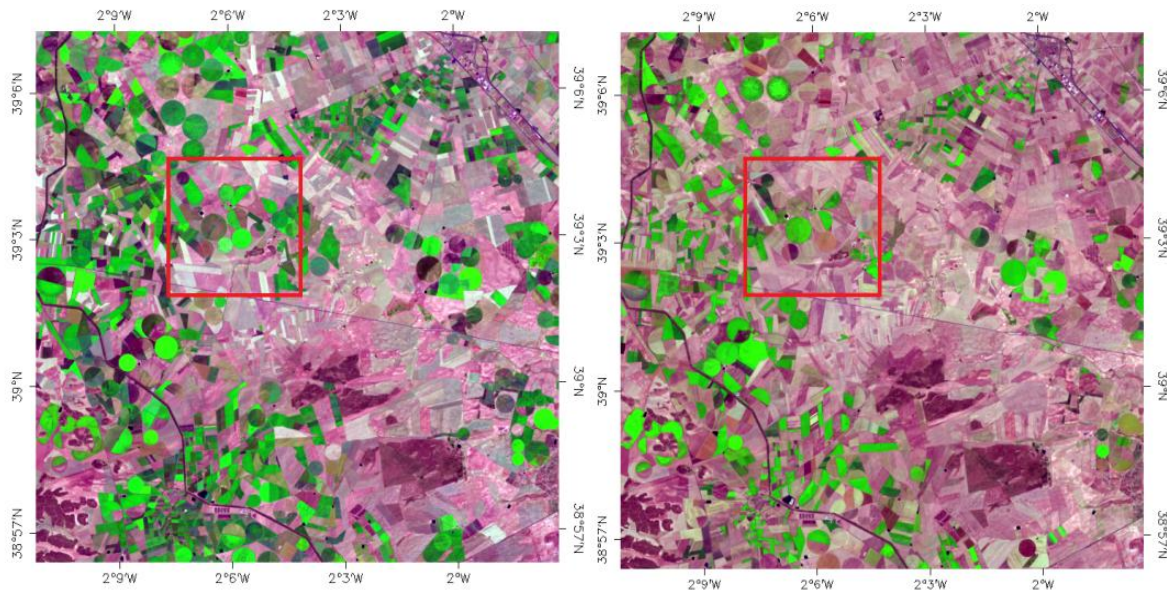


Figure 3: False color composition (RGB – SWIR-NIR-RED) of TOC Reflectance Landsat-8 images over the study area 20 km². (Barrax, 07th June (left) and 16th July (right), 2015). The red square outlines the 5 km² area of interest.

3.2. DESCRIPTION OF THE TEST SITE

The area is characterized by a flat morphology and large uniform land-use units, surrounded by large areas of cereals. Differences in elevation range up to 2 m only.

The climatic conditions are in line with the typical Mediterranean features: high precipitations in spring and autumn and the minimum in summer. The annual rainfall averages is about 400 mm. Furthermore, the region has high thermal oscillations during all seasons. La Mancha represents one of the driest regions of Europe. The region consists of approximately 65% dry land and 35% irrigated land with different agricultural fields.

Due to the ideally conditions of *Las Tiesas - Barrax* site for remote sensing purposes (flat terrain, regularly clear skies, and controlled crops grown), several scientific campaigns founded by the European Space Agency (DAISEX, SEN2FLEX, SEN3EXP) have been conducted in the past.

The area around Barrax has been used for agricultural research for many years. Among the irrigated fields we found Corn, Wheat, Barley, Camelina, Onion, Garlic, Potato, Wheat and Sunflower among other crop types in minor proportion (e.g., vineyard, fruit trees, papaver). Figure 4 shows the land use map during the field campaigns (winter and spring seasons).

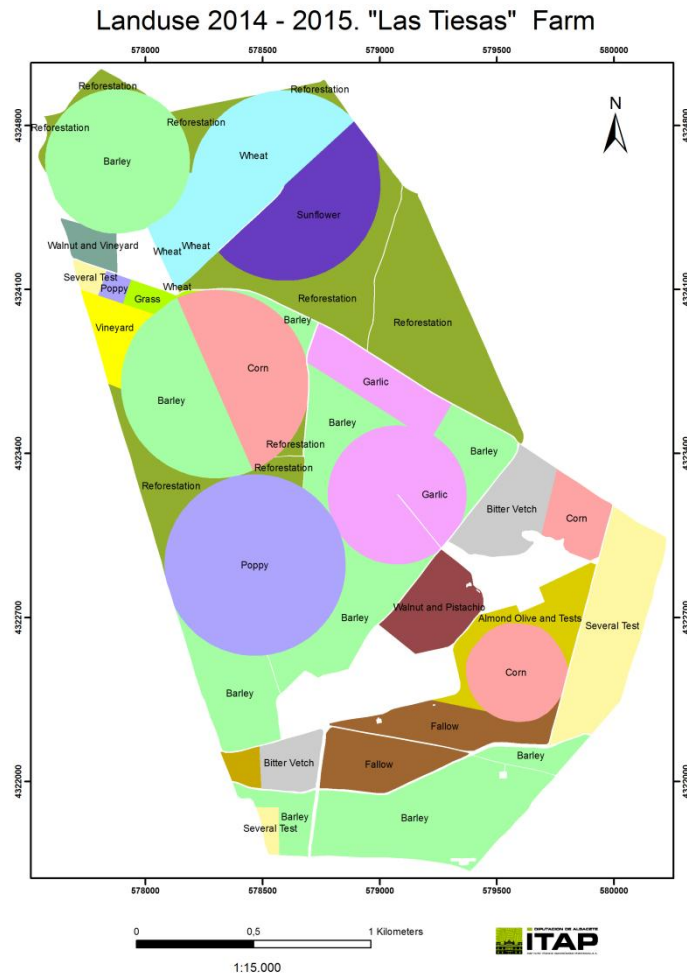


Figure 4: Land use map (winter and spring seasons) of *Las Tiasas* - *Barrax* (Spain).

Figure 5 shows some examples of crops in May 2015. These crop types are well representative of the crops of the region.

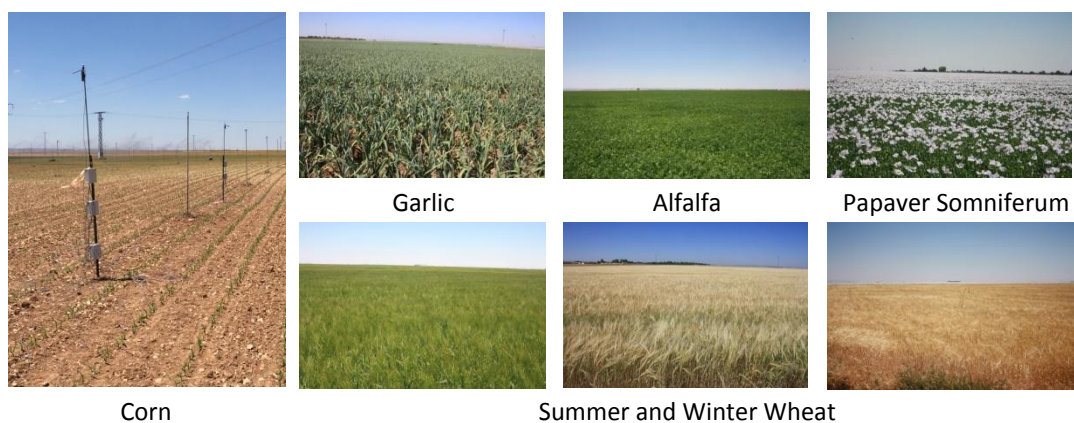


Figure 5: Pictures taken during the first field campaign (May, 2015) in *Las Tiasas* - *Barrax* (Spain).

4. GROUND MEASUREMENTS

The ground measurement database reported here was acquired by EOLAB.

4.1. MATERIAL AND METHODS

Several devices were used for estimating biophysical variables in the study area, including hemispherical digital photography (DHP), ceptometer (AccuPar LP-80) and LI-COR LAI 2200C plant canopy analyser.

4.1.1 Digital Hemispheric Photographs (DHP)

DHP were acquired with a digital camera. Hemispherical photos allow the calculation of LAI, FAPAR and FCOVER measuring gap fraction through an extreme wide-angle camera lens (i.e. 180°) (Weiss et al., 2004). It produces circular images that record the size, shape, and location of gaps, either looking upward from within a canopy or looking downward from above the canopy. The used system is composed by a professional camera and a fisheye lens: CANON EOS 6D and a SIGMA 8mm F3.5 – EX DG.

Since optical systems are not perfect, it is needed to calibrate the system in order to determinate the Optical Centre and the Projection Function (Weiss, 2010). The optical centre is defined by the projection of the optical axis onto the CCD matrix where the image is recorded, for our dual system (camera and lens) was found in the point: (x=1378, y=896) (Latorre et al. 2014).

The hemispherical photos acquired during the field campaign were processed with the CAN-EYE software version 6.4 (developed by INRA <http://www6.paca.inra.fr/can-eye>) to derive LAI, FAPAR and FCOVER. It is based on a RGB colour classification of the image to discriminate vegetation elements from background (i.e., gaps). This approach allows exploiting downward-looking photographs for short canopies (background = soil) as well as upward-looking photographs for tall canopies (background = sky). CAN-EYE software processes simultaneously up to of 20 images acquired over the same ESU. Note that our images were acquired with similar illumination conditions to limit the variation of colour dynamics between images.

The processing is achieved in 3 main steps (Weiss et al., 2004). First, image pre-processing is performed, which includes removing undesired objects (e.g. operator, sun glint) and image contrast adjustments to ensure a better visual discrimination between vegetation elements and background. Second, an automatic classification (k-means clustering) is applied to reduce the total number of distinctive colours of the image to 324 which is sufficient to ensure accurate discrimination capacities while keeping a small enough number of colours to be easily manipulated. Finally, a default classification based on predefined colour segmentation is first proposed and then iteratively refined by the user. The allocation of the colours to each class (vegetation elements versus background) is the most critical phase that needs to be interactive because colours depend both on illumination conditions

and on canopy elements. At the end of this process a binary image, background versus vegetation elements (including both green and non-green elements) is obtained.

The CAN-EYE software computes biophysical variables from gap fraction as follows:

Effective LAI (LAI_{eff}): Among the several methods described in Weiss et al (2004), the effective LAI estimation in the CAN-EYE software is performed by model inversion. The effective LAI is estimated from the Plant Area Index (PAI) which is the variable estimated by CAN-EYE, as no distinction between leaves or other plant elements are made from the gap fraction estimates. PAI is very close to the effective LAI for croplands when pictures are taken downward looking, whereas larger discrepancies are expected for forest when pictures are taken upward looking. Effective LAI is directly retrieved by inverting Eq. (1) (Poisson model) and assuming an ellipsoidal distribution of the leaf inclination using look-up-table (LUT) techniques.

$$P_0(\theta_v, \varphi_v) = e^{-N \cdot (\theta_v, \varphi_v)} = e^{-G \cdot (\theta_v, \varphi_v) \cdot \frac{LAI_{eff}}{\cos(\theta_v)}} \quad \text{Eq. (1)}$$

A large range of random combinations of LAI (between 0 and 10, step of 0.01) and ALA (Average Leaf Angle) (10° and 80°, step of 2°) values is used to build a database made of the corresponding gap fraction values (Eq.1) in the zenithal directions defined by the CAN-EYE user (60° for the DHP collection in this field campaign). The process consists then in selecting the LUT element in the database that is the closest to the measured P_0 . The distance (cost function C_k) of the k^{th} element of the LUT to the measured gap fraction is computed as the sum of two terms. The first term computes a weighted relative root mean square error between the measured gap fraction and the LUT one. The second term is the regularization term that imposes constraints to improve the PAI estimates. Two equations are proposed for the second “regularization” term:

(1) constraint used in CAN-EYE V5.1 on the retrieved ALA values that assume an average leaf angle close to $60^\circ \pm 03^\circ$, and

(2) constraint used in CAN-EYE V6.1 on the retrieved PAI value that must be close from the one retrieved from the zenithal ring at 57°. This constraint is more efficient, but it can be computed only when the 57° ring is available (i.e., $COI \geq 60^\circ$)

The software also proposed other ways of computing PAI and ALA effective using Miller's formula (Miller, 1967) which assumed that gap fraction only depends from view zenith angle. Furthermore, the CAN-EYE makes an estimation using the Welles and Norman (1991) method used in LAI-2000 for 5 rings. These LAI2000-like estimates were not used here as are based on the same Miller's formula but using limited angular sampling.

LAI: The actual LAI that can be measured only with a planimeter with however possible allometric relationships to reduce the sampling, is related to the effective leaf area index through:

$$LAI_{eff} = \lambda_0 \cdot LAI \quad \text{Eq. (2)}$$

where λ_0 is the clumping index. In CAN-EYE, the clumping index is computed using the Lang and Xiang (1986) logarithm gap fraction averaging method, although some uncertainties are associated to this method (Demarez et al., 2008). The principle is based on the assumption that vegetation elements are locally assumed randomly distributed. Values of clumping index given by CAN_EYE are in certain cases correlated with the size of the cells used to divide photographs. The values reported here were estimated with an average of the three results (CEV6.1, CEV5.1 and Miller).

As the CAN-EYE software provides different results (CEV6.1, CEV5.1 and Miller's) for LAI_{eff} and LAI variables; an average LAI value was provided as ground estimate, and the standard deviation of the different method LAI estimates was reported as the uncertainty of the estimate (see associated 2015_VGM_LasTiasas_Barrax.xls file). Note that for LAI, only CEV6.1 and CEV5.1 were used.

FCOVER is retrieved from gap fraction between 0 to 10°.

$$FCOVER = 1 - P_0 \cdot (0 - 10^\circ) \quad \text{Eq. (3)}$$

FAPAR: As there is little scattering by leaves in that particular spectral domain due to the strong absorbing features of the photosynthetic pigments, FAPAR is often assumed to be equal to FIPAR (Fraction of Intercepted Photosynthetically Active Radiation), and therefore directly related to the gap fraction. The actual FAPAR is the sum of two terms, weighted by the diffuse fraction in the PAR domain: the 'black sky' FAPAR that corresponds to the direct component and the 'white sky' or the diffuse component.

The instantaneous "Black-sky FAPAR" ($FAPAR^{BS}$) is given at a solar position (date, hour and latitude). Depending on latitude, the CAN EYE software computes the solar zenith angle every solar hour during half the day (there is symmetry at 12:00). The instantaneous FAPAR is then approximated at each solar hour as 1 minus the gap fraction in the corresponding solar zenith angle:

$$FAPAR^{BS}(\theta_s) = 1 - P_0 \cdot (\theta_s) \quad \text{Eq. (4)}$$

The "daily integrated" black-sky FAPAR is computed as the following:

$$FAPAR_{Day}^{BS} = \frac{\int_{sunrise}^{sunset} \cos(\theta_s) \cdot [1 - P_0 \cdot (\theta_s)] \cdot d\theta}{\int_{sunrise}^{sunset} \cos(\theta_s) \cdot d\theta} \quad \text{Eq. (5)}$$

The "white-sky (or diffuse) FAPAR" is computed as the following:

$$FAPAR^{WS} = \frac{1}{\pi} \int_0^{2\pi} \int_0^\pi P_0 \cos(\theta_s) \sin(\theta_s) d\theta d\varphi = 2 \cdot \int_0^\pi P_0 \cos(\theta_s) \sin(\theta_s) d\theta \quad \text{Eq. (6)}$$

The CAN-EYE software provides the three FAPAR variables. Instantaneous black-sky FAPAR values at 10:00h SLT were up-scaled.

4.1.2 AccuPARLP80-Ceptometer

The AccuPAR model LP-80 (Figure 6) is a lightweight, portable, linear Photosynthetically Active Radiation (PAR) sensor (Decagon Devices, Inc. 2014). It lets you measure canopy PAR interception and calculate leaf area index (LAI) at any location within a plant or forest canopy. PAR data can be used with other climate data to estimate biomass production without destroying the crop. PAR is also important in determining other canopy processes; such as radiation interception, energy conversion, momentum, gas exchange, precipitation interception, and evapotranspiration.

It consists of an integrated microprocessor-driven data logger and probe. The probe contains 80 independent sensors, spaced 1 cm apart. The photo sensors measure PAR in the 400 to 700 nm waveband. The AccuPAR displays PAR in units of micro-mols per meter squared per second ($\mu\text{mol} \times \text{m}^{-2} \times \text{s}^{-1}$). The instrument is capable of hand-held or unattended measurement.



Figure 6: AccuPAR LP80-Ceptometer

For AccuPAR, the effective PAI is derived following the equations to predict the scattered and transmitted PAR (Norman and Welles, 1983).

$$PAI_{eff} = \frac{\left[\left(1 - \frac{1}{2k} \right) f_b - 1 \right] \ln \tau}{A(1 - 0.47 f_b)} \quad \text{Eq.(7)}$$

Where τ is the transmission coefficient obtained through the ratio of the below canopy and the above canopy PARs, f_b is the fraction of incident beam PAR, A is a function of the leaf absorptivity (a) in the PAR band (AccuPAR assumes $a = 0.9$, and $A=0.86$ in LAI sampling routines), and k is the extinction coefficient for the canopy. K coefficients for typical crops are provided in the manual. It can be estimated as the ratio between the height and the width of the plant. We have used a range of values between 0.8 and 1.4 depending on the type and status of the canopy.

4.1.3 LI-COR LAI-2200C plant canopy analyser

The LAI-2200C (LI-COR Inc., Lincoln, Nebraska, 2013) is a model of plant canopy analyser used in the field campaign (Figure 7).



Figure 7: LAI-2200C device.

This instrument calculates Leaf Area Index (LAI) and other canopy attributes from light measurements made with a “fish-eye” optical sensor (148° field-of-view). Measurements made above and below the canopy are used to calculate canopy light interception at five zenith angles (Figure 8). The average probability of light penetration into the canopy is computed by

$$\overline{P(\theta_i)} = \frac{1}{N_{obs}} \sum_{j=1}^{N_{obs}} \frac{B_{ij}}{A_{ij}} \quad \text{Eq. (8)}$$

where the subscript i ($i = 1 \dots 5$) refers to the optical sensor rings centered at θ_i and j refers to the number of observational pairs ($j = 1 \dots N_{obs}$). B_{ij} and A_{ij} are the j^{th} below and above canopy readings, respectively, for the i^{th} ring. The gap fraction for the i^{th} ring is computed from

$$G_i = e^{\left(\overline{\ln P(\theta_i)}\right)} = e^{\left(\frac{1}{N_{obs}} \sum_{j=1}^{N_{obs}} \ln \frac{B_{ij}}{A_{ij}}\right)} \quad \text{Eq. (9)}$$

Assuming the foliage elements are randomly distributed in space, the effective PAI (PAI_{eff}) can be estimated by the transmittance in the different view angles based on Miller's formula (Miller, 1967).

$$PAI_{eff} = 2 \int_0^{\pi/2} -\ln P(\theta) \cos \theta \sin \theta d\theta \quad \text{Eq. (10)}$$

The amount of foliage in a vegetative canopy can be deduced from measurements of how quickly radiation is attenuated as it passes through the canopy. By measuring this attenuation at several angles from the zenith, foliage orientation information can also be obtained. The LAI-2200 measures the attenuation of diffuse sky radiation at five zenith angles simultaneously, arranged in concentric rings.

A normal measurement with the LAI-2200 consists of a minimum of ten numbers: five of the numbers are the signals from the five detectors when the optical sensor was above the

vegetation, and the remaining five are the readings made with the sensor below the vegetation. For both readings, the sensor is looking up at the sky. Five values of canopy transmittance are calculated from these readings by dividing corresponding pairs.

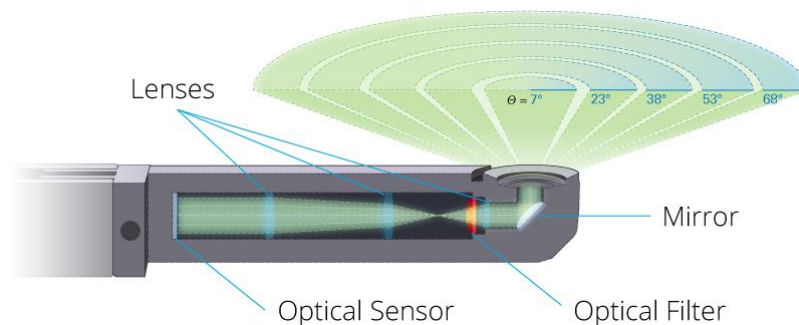


Figure 8: LAI-2200 optical sensor with 5 zenith angles

4.2. SPATIAL SAMPLING SCHEME

A pseudo-regular sampling was used within each Elementary Sampling Unit (ESU) of approximately 20x20 m². The centre of the ESU was geo-located using a Global Positioning System (GPS). A total of 31 and 37 ESUs for first and second campaign respectively over different land cover types, were characterized (Figure 9). The number of hemispherical photos per ESU ranges between 12 and 15. In several ESUs, continuous measurements were taken with PASTIS-PAR devices for monitoring the seasonal cycle.



Figure 9: Distribution of the Elementary Sampling Units (ESU) over the study area of Las Tiesas - Barrax site. Left: First field campaign (27th May 2015). Right: Second field campaign (22nd July 2015). DHP, LAI2200C and LP80 sampling (orange and blue), visual inspection ESUs (white) and ground control points (red).

The spatial sampling (Figure 9) scheme was predefined to cover the existing variability over the study area. Additional elementary sampling units (ESU) were selected to complete the representation of the land cover types presented in the study area, such as Bare Soil (BS) and senescent crops where green values were estimated by visual inspection either because it corresponds to bare areas or to completely dry (i.e, Non-Photosynthetically active Vegetation, NPV). The proportion of bare areas and NPV crops was quite large (around 25% for first campaign and 36% for the second campaign based on NDVI threshold 0.16) in the study area during both field campaigns.

Figure 10 summarizes the distribution of the ESUs in the study area per each crop type acquired during the two field campaigns, where the percentage of each vegetation type sampled is shown. The more representative crops were: papaver, garlic, wheat, corn and alfalfa crops.

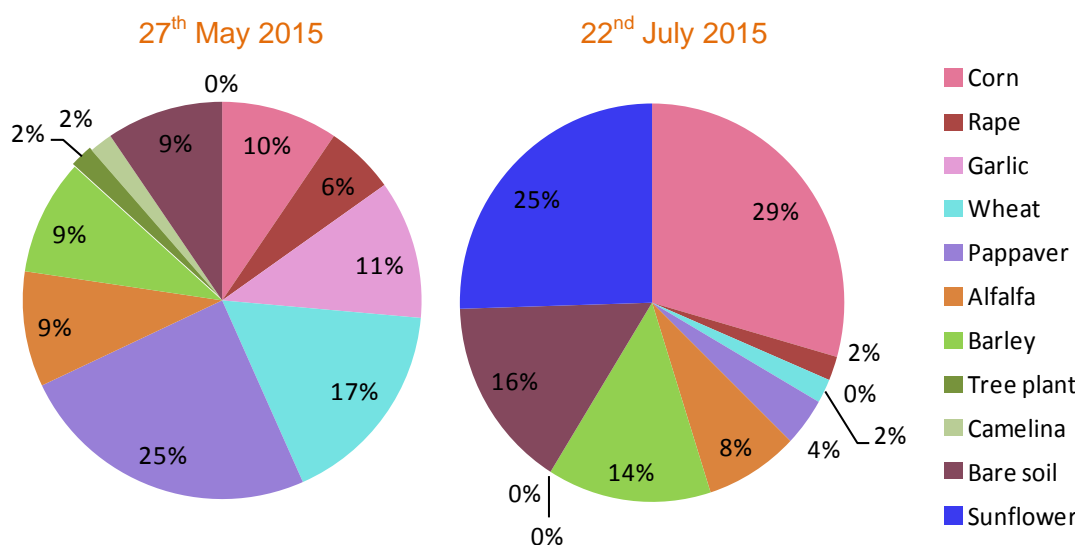


Figure 10: Distribution of vegetation types sampled during the field campaigns. *Las Tiesas – Barrax* site (Spain) 2015. Left: First field campaign (27th May). Right: Second field campaign (22nd July).

4.3. GROUND DATA

4.3.1. Data processing

The software CAN-EYE version V 6.4 was used to process the DHP images. Figure 11 shows some examples of DHP over several ESUs. Note the low vegetated coverage of the corn fields during the first campaign (Top) as compared with the second campaign (Bottom).



Figure 11: Digital Hemispherical Photographs acquired in *Las Tiesas - Barrax* site (Spain) during the field campaigns in 2015. Top: First field campaign (27th May). Bottom: Second field campaign (22nd July).

Figure 12 shows an example of the CAN-EYE processing results carried out on a Garlic crop ESU (Garlic G1-ESU14) during the first field campaign (27th May, 2015). Different results of the CAN-EYE processing are selected: the classification of vegetation (a) and the image generated by the software (b). Other graphs are shown: the average gap fraction (c) and the clumping factor versus view zenith angle (d).

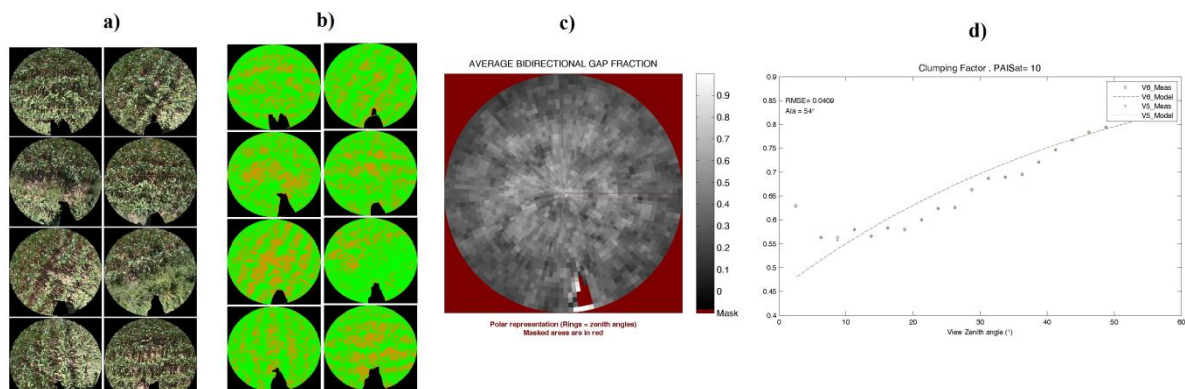


Figure 12: Results of the CAN-EYE processing carried out on a Garlic crop ESU (Garlic G1 - ESU 14) during the first field campaign (27th May, 2015). (a) DHP images. (b) Classified images. (c) Average gap fraction and (d) the clumping factor versus view zenith angle.

As described in section 4.1, CAN-EYE provides the LAI and effective LAI values by using three different methods: CEV6.1, CEV5.1 and Miller's. Figure 13 and Figure 14 show the

inter-comparison between the three methods. For LAleff, the results are very similar and the average of the three estimations is provided on the ground dataset. However for the LAI, the scattering between methods is much higher for medium values, displaying Miller's method lowest estimations than CEV6.1 and CEV5.1. It can be explained that the Miller's method does not consider all the viewing angles, and it has been discarded for the LAI average in the ground dataset.

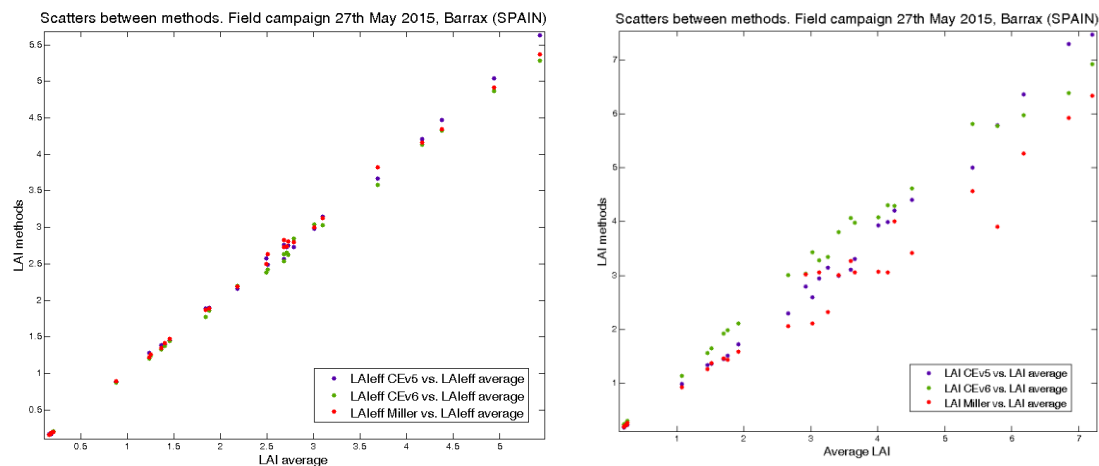


Figure 13: Inter-comparison of the calculated biophysical variables LAI (left side) and LAleff (right side) over the ESUs with different methods: CEV5.1, CEV6.1 and Miller's formula. Las Tiesas site – Barrax (Spain) during the campaign of 27th May, 2015.

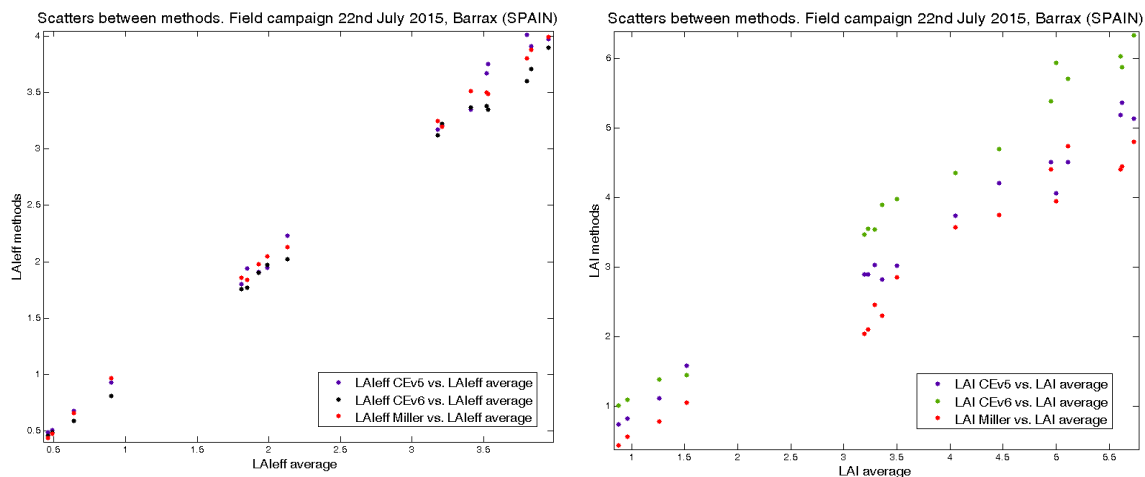


Figure 14: Inter-comparison of the calculated biophysical variables LAI (left side) and LAleff (right side) over the ESUs with different methods: CEV5.1, CEV6.1 and Miller's formula. Las Tiesas site – Barrax (Spain) during the campaign of 22nd July, 2015.

Figure 15 shows the intercomparison between LAI and effective LAI with instantaneous FAPAR at 10:00 SLT. The typical positive exponential curve is observed, most clearly for LAI for the first campaign, and for the LAI_{eff} for the second one.

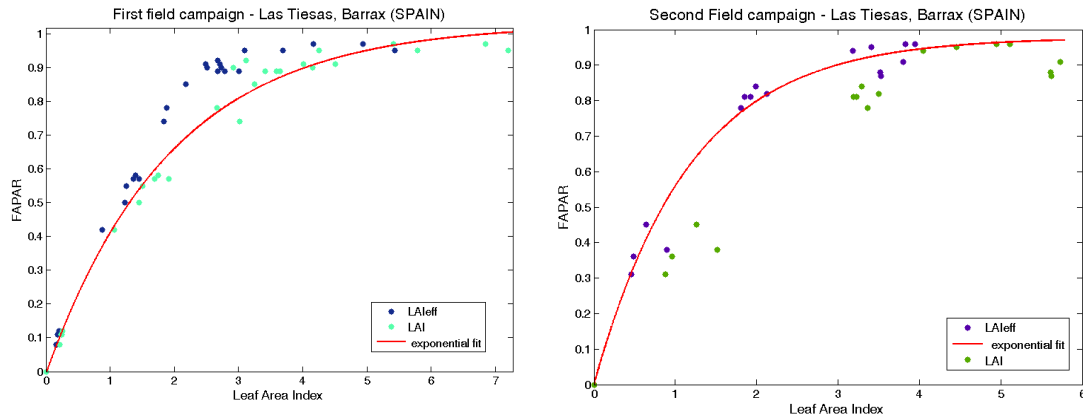


Figure 15: Intercomparison of the measured biophysical variables over the ESUs. Effective LAI and LAI versus FAPAR, Las Tiesas site – Barrax (Spain). Left side: First field campaign (27th May). Right side: Second field campaign (22nd July).

Figure 16 shows the intercomparison between FAPAR and FCOVER, the typical linear relationship is observed. ESUs with differences between FAPAR and FCOVER values upper than 0.25 were marked as suspicious in the ground dataset (Figure 16, orange dots).

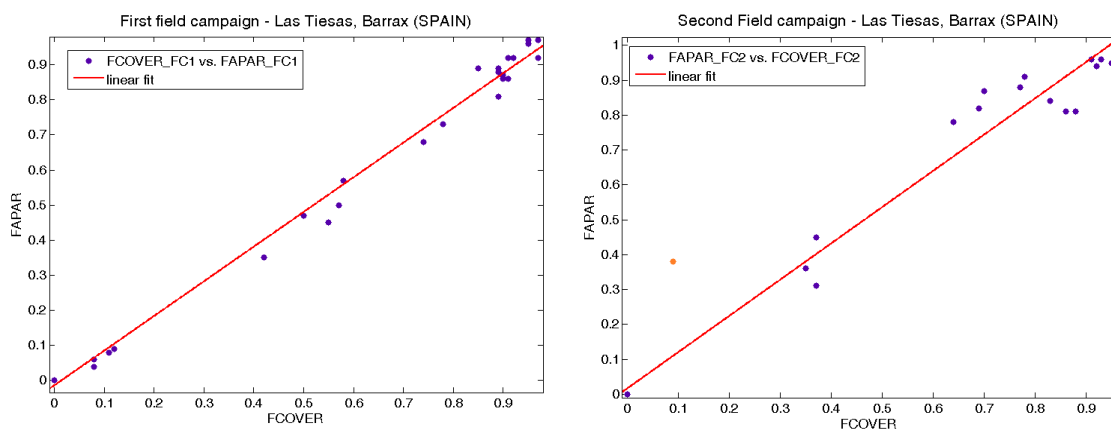


Figure 16: Intercomparison of the measured biophysical variables over the ESUs. FAPAR versus FCOVER, Las Tiesas site – Barrax (Spain). Left side: First field campaign (27th May). Right side: Second field campaign (22nd July).

Special cases:

We have found in some ESUs displaying very homogeneous and complete coverage a lower clumping index than expected. Figure 17 shows two examples for Alfalfa (ESU26) and Papaver (ESU10) where the clumping index values should be close to 1 (i.e. non clumped vegetation) but the CAN-EYE provides a clumping index around 0.7. For these special cases (very homogeneous plant cover) the clumping index has been set to 0.95 in the ground dataset.

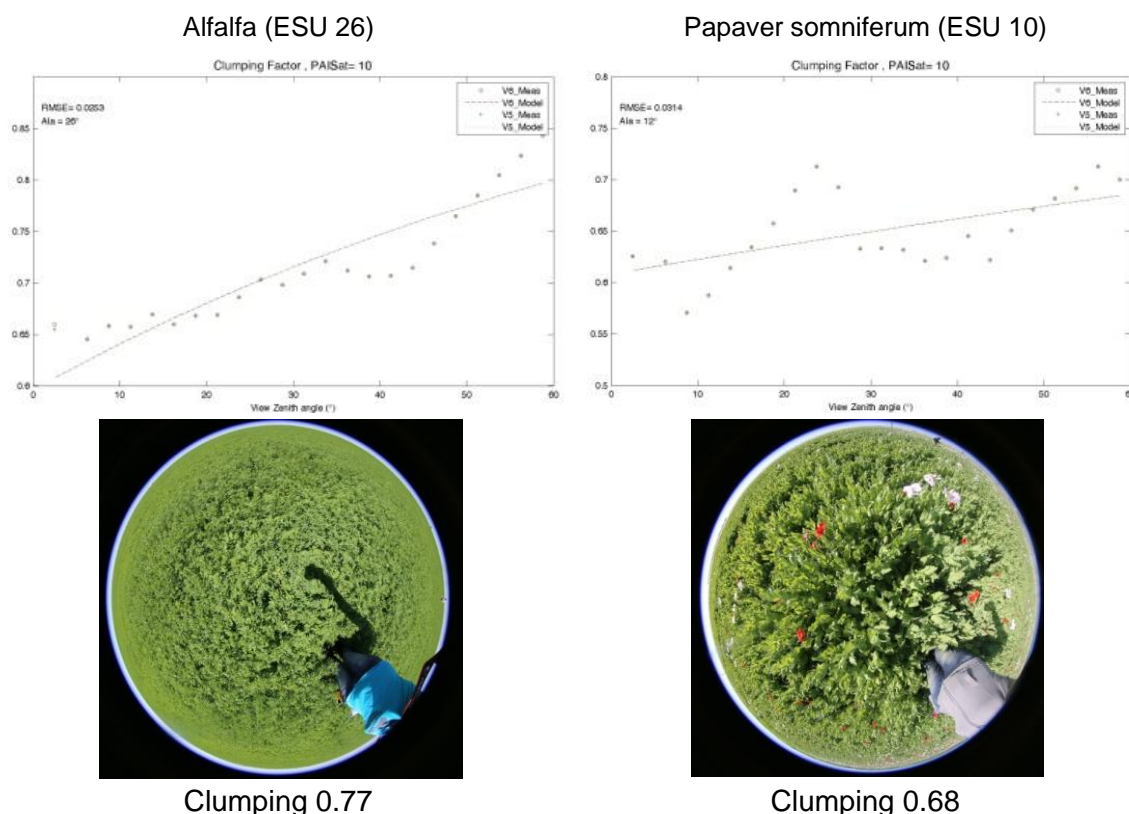


Figure 17: Results of the clumping processing by CAN-EYE carried out on two ESUs during the first field campaign (27th May 2015), Barrax. Left side: ESU 21, wheat field. Right side: ESU 10, papaver somniferum field.

Moreover, for the very homogeneous alfalfa and papaver covers, the acquisition should be taken from above (downward looking) in order to not modify the state of the vegetation canopy. Indeed, the camera disturbs the natural state of the plant canopy and opens a large gap fraction around the zenith, which can introduce an important underestimation mainly in the vegetation cover fractions (ImagineS report, Latorre et al., 2015). The clumping index would be also affected (lower values) as the angular distribution of the gap fraction will be also disturbed.

4.3.2. Content of the Ground Dataset

Each ESU is described according to a standard format. The header of the database is shown in Table 2.

Table 2: The Header used to describe ESUs with the ground measurements.

Column	Var.Name	Comment
1	Plot #	Number of the field plot in the site
2	Plot Label	Label of the plot in the site
3	ESU #	Number of the Elementary Sampling Unit (ESU)
4	ESU Label	Label of the ESU in the campaign
5	Northing Coord.	Geographical coordinate: Latitude (°), WGS-84
6	Easting Coord.	Geographical coordinate: Longitude (°), WGS-84
7	Extent (m) of ESU (diameter)	Size of the ESU ⁽¹⁾
8	Land Cover	Detailed land cover
9	Start Date (dd/mm/yyyy)	Starting date of measurements
10	End Date (dd/mm/yyyy)	Ending date of measurements
11	Products*	Method
12		Nb. Replications
13		PRODUCT
14		Uncertainty
		Instrument
		Number of Replications
		Methodology
		Standard deviation

*LAI_{eff}, LAI, FAPAR and FCOVER

Figure 18 to Figure 21 show the biophysical parameters obtained during the field experiment. Note that for all variables, additional ESU control points (ECP) were included in order to extend the sampling over bare areas or senescent crops (non photosynthetically active), completely dry. LAI, FAPAR and FCOVER was set to zero in these ECP locations (See Annex I).

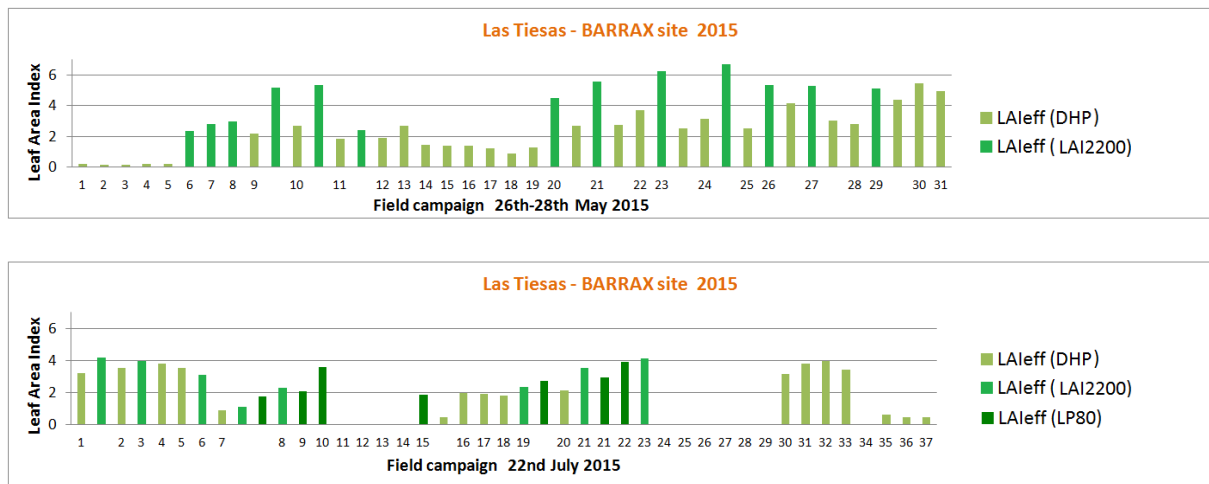


Figure 18: LAleff measurements acquired in Las Tiesas site – Barrax, during the field campaigns, 2015. Top: first campaign, 26th – 28th May. Bottom: second campaign, 22nd July.

Figure 18 shows the effective LAleff, ranging between 0.16 (corn crops, ESUs 1 to 5) and 6.7 (papaver crops, ESUs 9 to 13 (field P1) and 23 to 25 (field P2)) for the first campaign and between 0 (senescent harvested fields) to around 4 over corn crops (ESUs 1 to 10 (fields C1 and C2)) for the second one. Lower values were obtained for Corn in early stages of growth for the first campaign and harvested.

Maximum values were obtained for the Barley field (ESUs 29 to 31) and for the papaver *Somniferum*. Rape, Barley and Wheat crops presented also higher values (first campaign). The higher values for the second campaigns belong mainly to alfalfa (ESUs 30 to 33) and corn crops.

Over some ESUs, different instrumentations were used: DHP, LAI2200 and LP80. For this reason, for LAleff measurement, the x axis presents duplicated values (Figure 18) (See Annex I). In general, the DHP measurements are lower than the measures acquired with other devices, in particular with LAI-2200. Larger discrepancies were observed over Papaver field (ESU 23, ESU 24) in the first field campaign. These discrepancies can be attributed to the different sampling (downward looking with DHP, upward looking with LAI-2200). Using the DHP, the shaded layers at the bottom of the canopy are not considered, whereas the LAI-2200 measured the intercepted radiation by all elements (and layers) in the canopy. The different FOV of the devices and spatial sampling can introduce additional differences, as the DHP captures larger areas than LAI-2200C.

Similar distributions were obtained for LAI (Figure 19), with higher values due to the clumping factor. Some homogeneous and dense vegetation, such as alfalfa or papaver, presented underestimated clumping index values and we have adjusted them to 0.95 (See Special Cases and Figure 17).

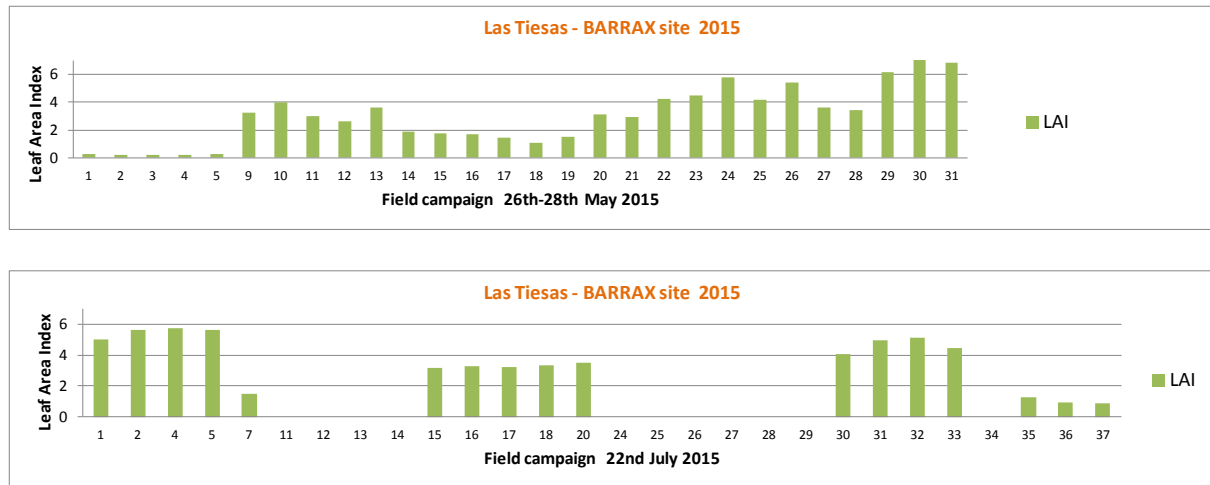


Figure 19: As in Figure 18 for LAI

Figure 20 shows the FAPAR (instantaneous at 10:00 SLT and daily integrated) values covering approximately the full dynamic range for the first field campaign, with minimum values for corn (0.08), medium to high absorption values for garlic, around 0.6 (i.e. ESU 14, with 0.57 for instantaneous and 0.62 for FAPAR daily integrated). The values for the second field campaign are close to 0.9 for the most of crops minus harvested and senescent fields, and one sunflower field (SF2, ESUs 35 to 37). The corn field C2 (ESUs 7, 8 and 9) presented lower values because the plants were partially dry.

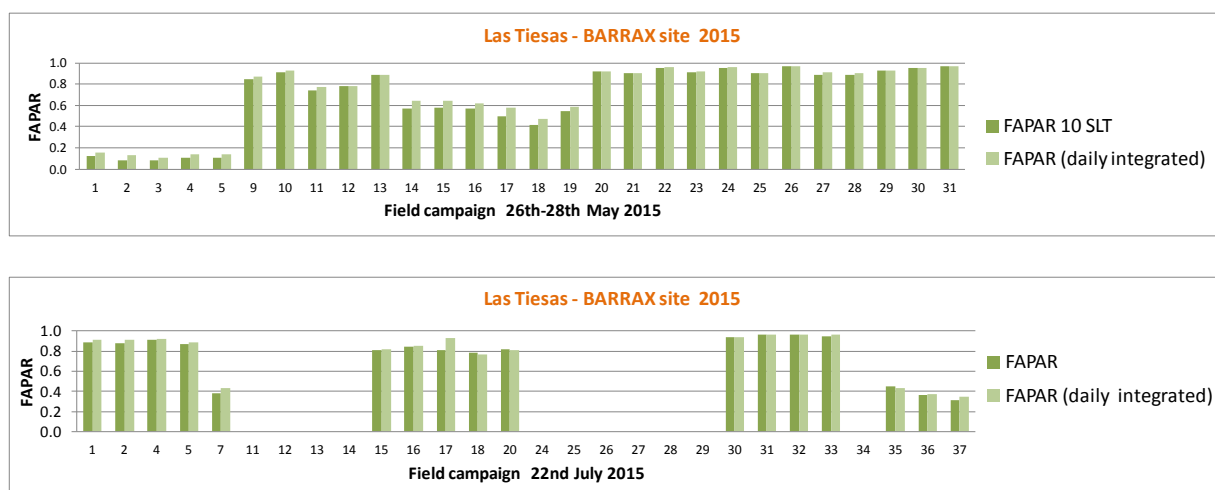


Figure 20: As in Figure 18 for FAPAR 10:00 SLT and daily integrated FAPAR

Very similar results were found between FAPAR daily integrated and instantaneous at 10:00 SLT, but slightly lower for the instantaneous values at 10:00 SLT. As we obtained similar values for instantaneous FAPAR at 10:00 SLT and daily FAPAR integrated

observations, only one map of FAPAR product has been provided (from the instantaneous values).

Figure 21 shows the FCOVER variable, quite similar to FAPAR, full cover was obtained for alfalfa and papaver for the first field campaign. Some measurements were not consistent with the reflectivity of the TOC image (11 days taken after the first field campaign) and they have not been taken into account for up-scaling, (i.e., ESUs 14 to 16 for alfalfa field).

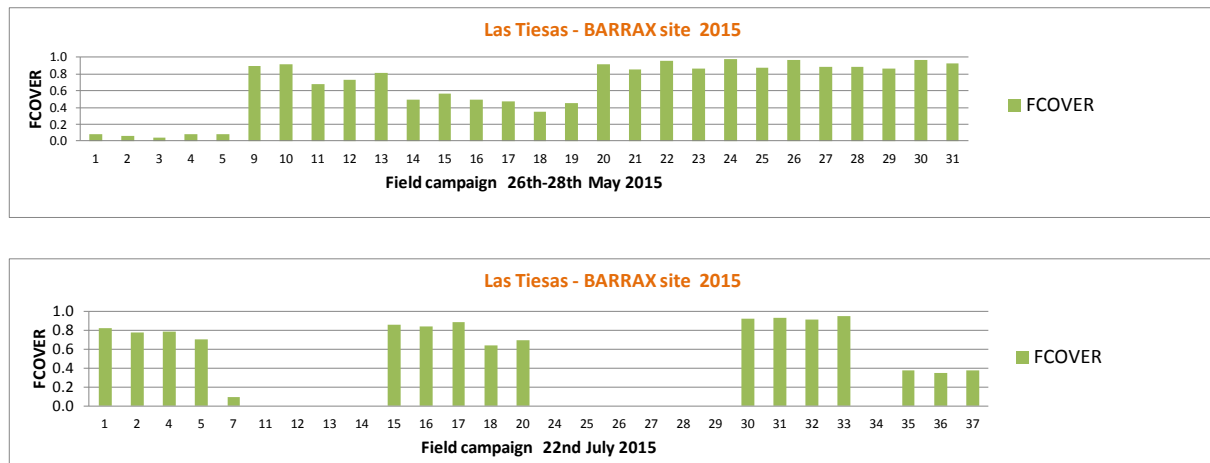


Figure 21: As in Figure 18 for FCOVER

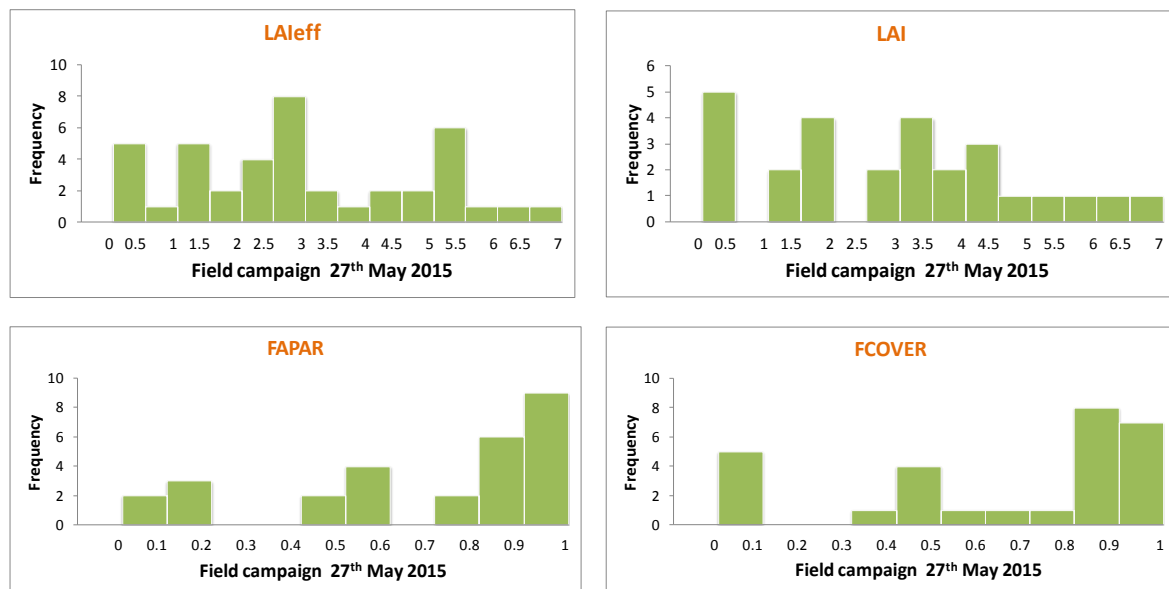


Figure 22: Distribution of the measured biophysical variables over the ESUs, Las Tiesas site – Barrax, during the first campaign on 27th May, 2015.

The values of FCOVER equal to zero, for the second campaign, correspond to non vegetated areas, harvested fields: papaver (ESUs 11 and 34), barley (ESUs 12, and 24 to 29), rape (ESU 13) and wheat (ESU 14) also sampled during the first campaign when it reached maximum values.

The distribution of the measured variables is presented in Figure 22 and Figure 23. Note that the larger frequencies are obtained for lowest variable values for the second campaign (summer 2015) due to senescent and harvested fields.

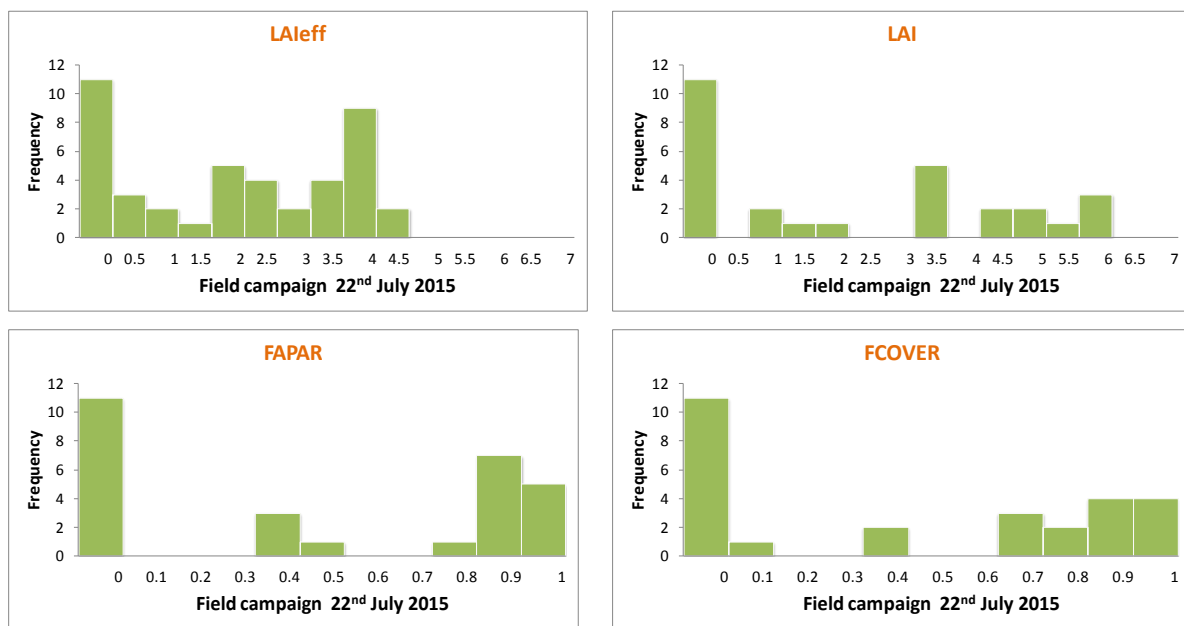


Figure 23: Distribution of the measured biophysical variables over the ESUs, Las Tiesas site – Barrax, during the second campaign on 22nd July, 2015.

5. EVALUATION OF THE SAMPLING

5.1. PRINCIPLES

Based on previous field activities, the data set sampling was concentrated in the most representative areas. The number of sampling points (included ESUs, ESU control points (ECP) and ground control points (GCP)) was 55 and 51, although only 31 and 37 ESUs were used for up-scaling, for the first and second field campaign respectively; and the others have been used to test the maps over problematic fields as bare or senescent areas.

5.2. EVALUATION BASED ON NDVI VALUES

The sampling strategy is evaluated using the Landsat-8 image by comparing the NDVI distribution over the site with the NDVI distribution over the ESUs (Figure 24). As the number of pixels is drastically different for the ESU and whole site (WS), it is not statistically consistent to directly compare the two NDVI histograms. Therefore, the proposed technique consists in comparing the NDVI cumulative frequency of the two distributions by a Monte-Carlo procedure which aims at comparing the actual frequency to randomly shifted sampling patterns. It consists in:

1. computing the cumulative frequency of the N pixel NDVI that correspond to the exact ESU locations; then, applying a unique random translation to the sampling design (modulo the size of the image)
2. computing the cumulative frequency of NDVI on the randomly shifted sampling design
3. repeating steps 1 and 2, 199 times with 199 different random translation vectors.

This provides a total population of $N = 199 + 1$ (actual) cumulative frequency on which a statistical test at acceptance probability $1 - \alpha = 95\%$ is applied: for a given NDVI level, if the actual ESU density function is between two limits defined by the $N\alpha/2 = 5$ highest and lowest values of the 200 cumulative frequencies, the hypothesis assuming that WS and ESU NDVI distributions are equivalent is accepted, otherwise it is rejected.

Figure 24 shows that the NDVI TOC distribution during the Barrax multi-temporal field campaigns is good over the whole site ($20 \times 20 \text{ km}^2$) for the two field campaigns. For the second campaign (22nd July, 2015) a slight bias toward lower NDVI values is appreciated.

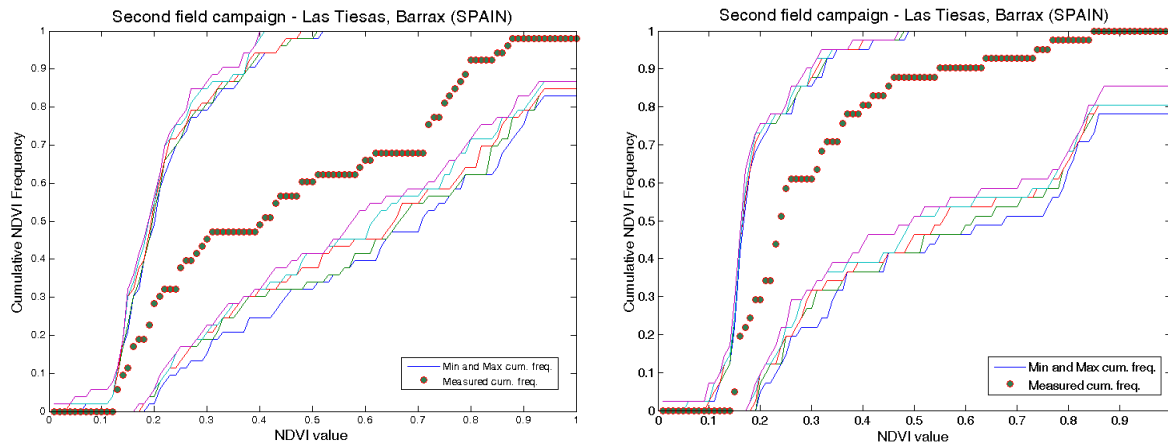


Figure 24: Comparison of NDVI TOC distribution between ESUs (brown dots) and over the whole image (blue line). Las Tiesas – Barrax (2015). Left: First field campaign (27th May). Right: Second field campaign (22nd July).

5.3. EVALUATION BASED ON CONVEX HULL: PRODUCT QUALITY FLAG.

The interpolation capabilities of the empirical transfer function used for up-scaling the ground data using decametric images is dependent of the sampling (Martinez et al., 2009). A test based on the convex hulls was also carried out to characterize the representativeness of ESUs and the reliability of the empirical transfer function using the different combinations of the selected bands (green, red, NIR and SWIR) of the Landsat-8 image. A flag image is computed over the reflectances. The result on convex-hulls can be interpreted as:

- pixels inside the 'strict convex-hull': a convex-hull is computed using all the Landsat-8 reflectances corresponding to the ESUs belonging to the class. These pixels are well represented by the ground sampling and therefore, when applying a transfer function the degree of confidence in the results will be quite high, since the transfer function will be used as an interpolator;
- pixels inside the 'large convex-hull': a convex-hull is computed using all the reflectance combinations ($\pm 5\%$ in relative value) corresponding to the ESUs. For these pixels, the degree of confidence in the obtained results will be quite good, since the transfer function is used as an extrapolator (but not far from interpolator);
- pixels outside the two convex-hulls: this means that for these pixels, the transfer function will behave as an extrapolator which makes the results less reliable. However, having a priori information on the site may help to evaluate the extrapolation capacities of the transfer function.

Figure 25 shows the results of the Convex-Hull test (i.e., Quality Flag image) for the Las Tiesas - Barrax site over a 20x20 km² (left) and 5x5 km² (right) areas around the central coordinate site. The strict and large convex-hulls are high around the test site, 74% and 70%

over the 20x20 km² area and 81% and 80% for 5x5 km² area, first and second field campaign respectively (Table 3).

Table 3: Percentages of Convex hull results over the study areas (20x20 km² and 5x5 km²) in Barrax, 2015. Convex hull values: 0= extrapolation of TF, 1= strict convex hull and 2= large convex hull.

Field Campaign	Quality Flags (%)											
DATE	26 th to 28 th May, 2015						22 nd July, 2015					
Size	5x5 km ²			20x20 km ²			5x5 km ²			20x20 km ²		
Convex hull values	0	1	2	0	1	2	0	1	2	0	1	2
	19	62	19	26	49	25	20	71	9	29	57	13

Las Tiesas site – Barrax 2015

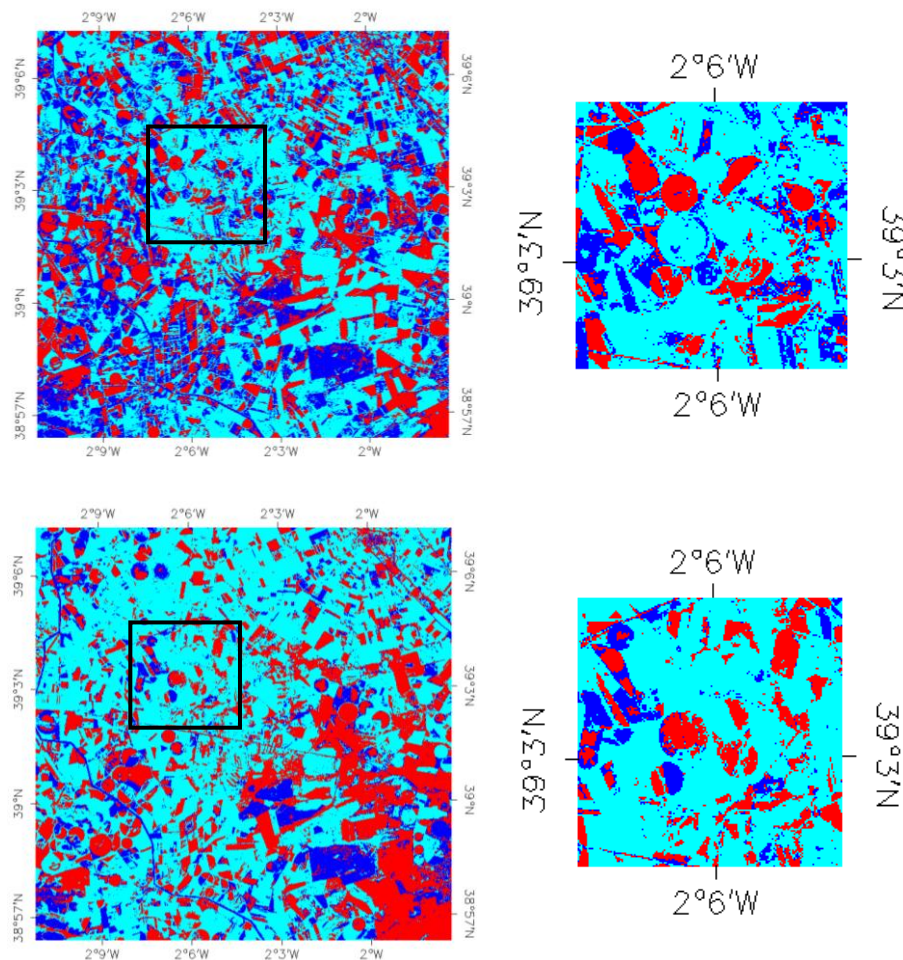


Figure 25: Convex Hull test over 20x20 km² (left side) and 5x5 km² (right side) areas: clear and dark blue correspond to the pixels belonging to the 'strict' and 'large' convex hulls. Red corresponds to the pixels for which the transfer function is extrapolating, Las Tiesas – Barrax, 2015. Top: First field campaign (27th May). Bottom: Second field campaign (22nd July).

6. PRODUCTION OF GROUND-BASED MAPS

6.1. IMAGERY

The Landsat-8 images were acquired the 7th June and 16th July, 2015 (Table 4 for acquisition geometry). We selected 4 spectral bands from 500 nm to 1750 nm with a nadir ground sampling distance of 30 m. For the transfer function analysis, the input satellite data used is Top of Canopy (TOC) reflectance. The original projection is UTM 30 North, WGS-84.

Table 4: Acquisition geometry of Landsat-8 data used for retrieving high resolution maps.

Landsat-8 METADATA		
Platform / Instrument	Landsat-8 / OLI_TIRS	
Path	199	200
Row	33	
Selected Bands	B3(green) : 0.53-0.59 μm B4(red) : 0.64-0.67 μm B5(NIR) : 0.85-0.88 μm B6(SWIR1) : 1.58-1.65 μm	
	First campaign	Second campaign
	26th to 28th May, 2015	22nd July, 2015
Acquisition date	2015.06.07	2015.07.16
	10:42:50	10:49:21
Illumination Azimuth angle	127.420°	126.763°
Illumination Elevation angle	23.572°	25.659°

6.2. THE TRANSFER FUNCTION

The measurements during the first campaign were collected eleven days before than the acquisition date of the Landsat-8 image used for the up-scaling. For this reason, some measurements provided in the ground dataset present inconsistent values with the TOC reflectance and NDVI values of the satellite image. These measurements, corresponding to fields of Alfalfa, Garlic (G1) and Wheat (W1), were not considered for the up-scaling.

6.2.1. The regression method

If the number of ESUs is enough, multiple robust regression 'REG' between ESUs reflectance and the considered biophysical variable can be applied (Martínez et al., 2009): we used the 'robustfit' function from the Matlab statistics toolbox. It uses an iteratively re-weighted least squares algorithm, with the weights at each iteration computed by applying the bi-square function to the residuals from the previous iteration. This algorithm provides lower weight to ESUs that do not fit well.

The results are less sensitive to outliers in the data as compared with ordinary least squares regression. At the end of the processing, two errors are computed: weighted RMSE (using the weights attributed to each ESU) (RW) and cross-validation RMSE (leave-one-out method) (RC).

As the method has limited extrapolation capacities, a flag image (Figure 25), based on the convex hulls, is included in the final ground based map in order to inform the users on the reliability of the estimates.

6.2.2. Band combination

Las Tiesas site – Barrax 26th – 28th May 2015

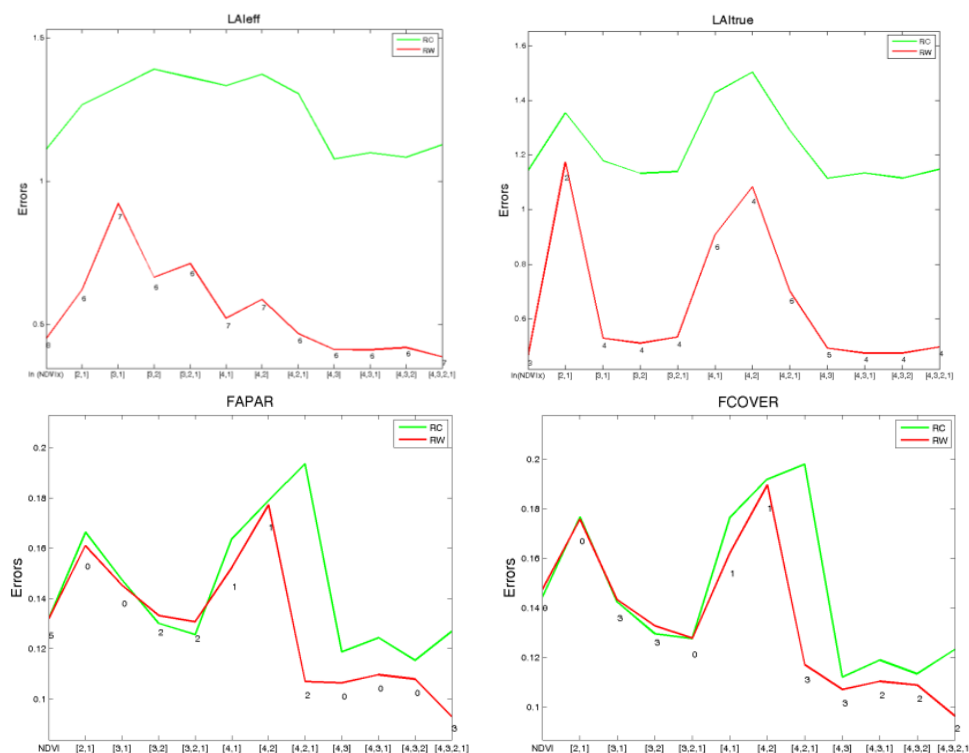


Figure 26: Test of multiple regression (TF) applied on different band combinations. Band combinations are given in abscissa (1=G, 2=RED, 3=NIR and 4=SWIR). The weighted root mean square error (RMSE) is presented in red along with the cross-validation RMSE in green. The numbers indicate the number of data used for the robust regression with a weight lower than 0.7 that could be considered as outliers. Barrax, first field campaign on 27th May 2015.

Figure 26 and Figure 27 show the errors (RW, RC) obtained for the several band combinations using TOC reflectance for the first and the second campaign, respectively. In this particular Barrax case, where the scene presents many senescent and harvested fields, we have selected the NDVI as input for the transfer function (exponential relationship with LA_{eff} and LAI, and linear relationship with FAPAR and FCOVER, see Section 6.2.3). NDVI shows, in all cases, lower errors over ESUs than 4-bands combination and assures good consistency of the maps over the whole area.

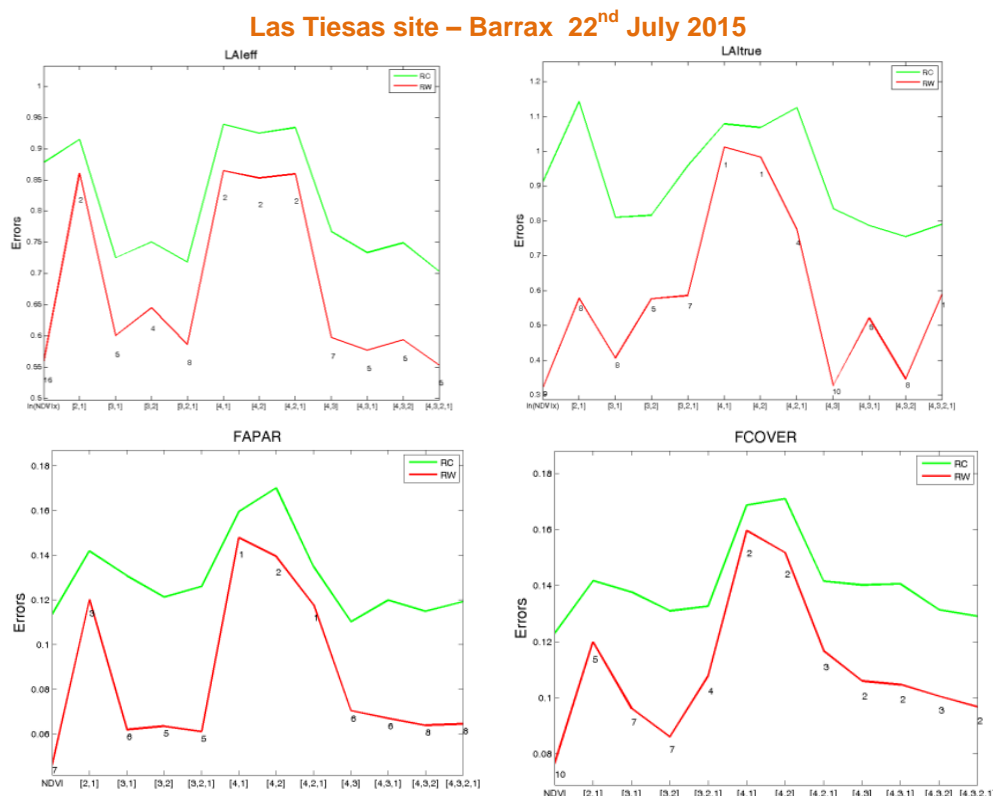


Figure 27: As in Figure 26 for the second campaign on 22nd July, 2015.

6.2.3. The selected Transfer Function

The applied transfer function is detailed in Table 5, along with its weighted (RW) and cross validated (RC) errors.

For the FAPAR and FCOVER, a simple linear relationship with NDVI was selected:

$$FAPAR = a + b \cdot NDVI \quad \text{Eq. (6)}$$

$$FCOVER = a + b \cdot NDVI \quad \text{Eq. (7)}$$

For the LA_{leff} and LAI, an exponential relationship with NDVI was selected according to Baret et al., (1989):

$$LA_{leff} = a + b \cdot \ln \left(\frac{NDVI_{\infty} - NDVI}{NDVI_{\infty} - NDVI_s} \right) \quad \text{Eq. (8)}$$

$$LAI = a + b \cdot \ln \left(\frac{NDVI_{\infty} - NDVI}{NDVI_{\infty} - NDVI_s} \right) \quad \text{Eq. (9)}$$

Where b represents the extinction coefficient which depends on the average leaf angle inclination, solar zenith angle and diffuse reflectance and transmittance of the leaves. “ b ” was set empirically with the ground data for each transfer function, as well as the residuals “ a ”. $NDVI_s$ represents the typical NDVI of bare soil areas and $NDVI_{\infty}$ represents the NDVI of fully developed canopies, both assumed to be constant over the image. $NDVI_s$ was set to 0.15 and $NDVI_{\infty}$ to 0.95.

Table 5: Transfer function applied to the whole site for LA_{leff}, LAI, instantaneous FAPAR at 10:00 SLT and FCOVER. RW for weighted RMSE, and RC for cross-validation RMSE. $NDVI_{\infty}$ corresponds to NDVI value for fully developed canopies, and $NDVI_s$ to NDVI value for bare soil areas.

Variable	Band Combination	RW	RC
27th May, 2015		First Campaign	
LA_{leff}	$-0.054 - 1.59 \cdot \ln \left(\frac{NDVI_{\infty} - NDVI}{NDVI_{\infty} - NDVI_s} \right)$	0.450	1.090
LAI	$-0.210 - 2.384 \cdot \ln \left(\frac{NDVI_{\infty} - NDVI}{NDVI_{\infty} - NDVI_s} \right)$	0.462	1.125
FAPAR	$-0.256 + 1.397 \cdot NDVI$	0.132	0.122
FCOVER	$-0.264 + 1.365 \cdot NDVI$	0.147	0.135
22nd July, 2015		Second Campaign	
LA_{leff}	$-0.042 - 2.355 \cdot \ln \left(\frac{NDVI_{\infty} - NDVI}{NDVI_{\infty} - NDVI_s} \right)$	0.357	0.846
LAI	$-0.038 - 2.762 \cdot \ln \left(\frac{NDVI_{\infty} - NDVI}{NDVI_{\infty} - NDVI_s} \right)$	0.564	0.896
FAPAR	$-0.229 + 1.490 \cdot NDVI$	0.046	0.113
FCOVER	$-0.217 + 1.423 \cdot NDVI$	0.077	0.121

Figure 28 and Figure 29 show scatter-plots between ground observations and their corresponding transfer function (TF) estimates for the selected bands combination (i.e. the NDVI). A good correlation is observed for the LA_{leff}, LAI, FAPAR and FCOVER with points distributed along the 1:1 line, with no mean bias and low RMSE values. Note that some overestimated points (TF values higher than ground data) were observed for ESUs 1 to 4

(see Figure 28, FAPAR) corresponding to corn (height of 20 cm and displaying 6 leaves at the date of the first field campaign). It is explained in the fact that the corn crops show a quick rise at the early stages, and the date of image acquisition is around a week later than the measurements.

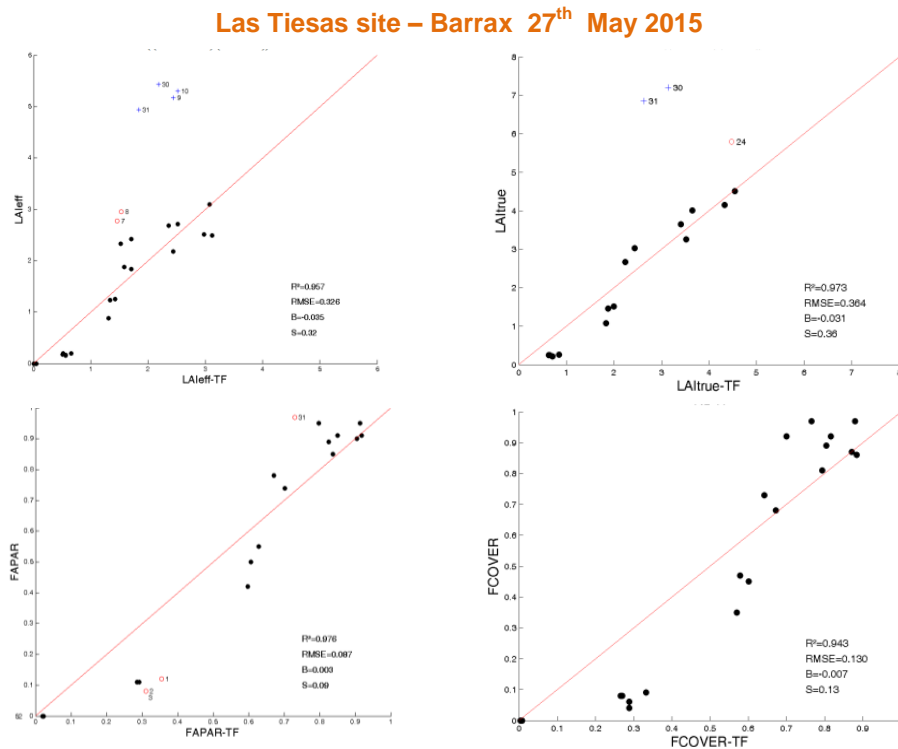


Figure 28: LAIeff, LAI, FAPAR and FCOVER results for regression on NDVI. Full dots: $Weight > 0.7$. Empty dots: $0 < Weight < 0.7$. Crosses: $Weight = 0$. Las Tiesas- Barrax, first field campaign 2015 on 27th May, 2015.

For the second campaign, the TF values for several ESUs of Corn (ESU 1 to 10) presented lower values than ground data, specially for LAIeff (see Figure 29, for LAIeff). On the contrary, overestimation of the TF values was detected for several sunflower fields in some ESUs (16 to 18) (Figure 20, LAIeff).

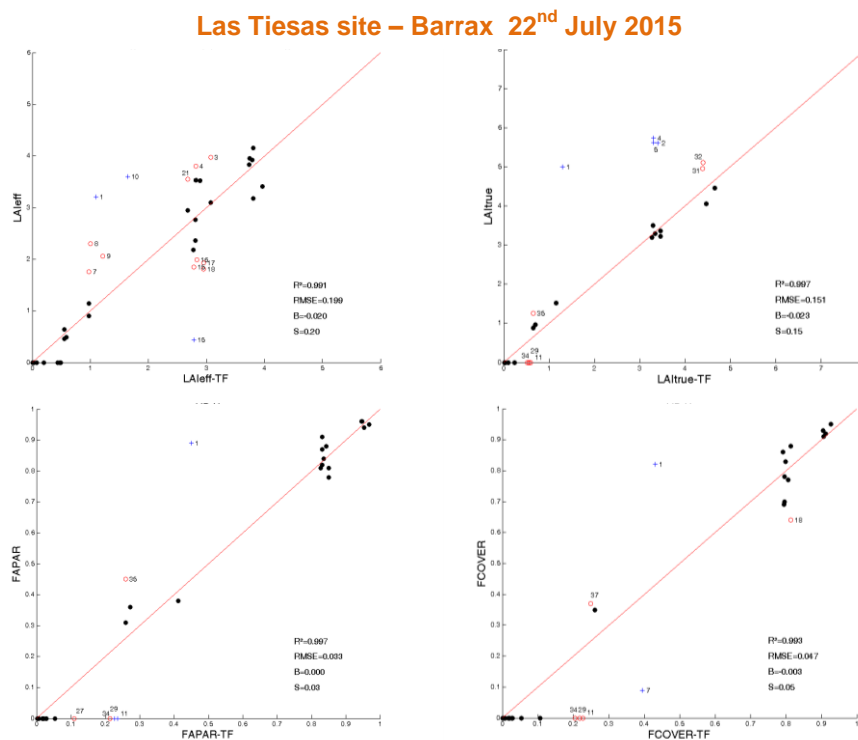


Figure 29: As Figure 28 for the second field campaign on 22nd July, 2015.

6.3. THE HIGH RESOLUTION GROUND BASED MAPS

The high resolution maps are obtained applying the selected transfer function (Table 5) to the Landsat-8 NDVI derived from TOC reflectances. The study area has been extended to 20x20km² (centre located at 39.028 N, 2.074 W, UTM zone 30 North, Datum WGS-84) covering the equivalent area than the ImagineS field experiment performed during the last 2014 year (ImagineS report, Latorre et al., 2015). Figure 30 to Figure 33 present the TF biophysical variables over the extended 20x20 km² area. Figure 25 shows the Quality Flag included in the final product.

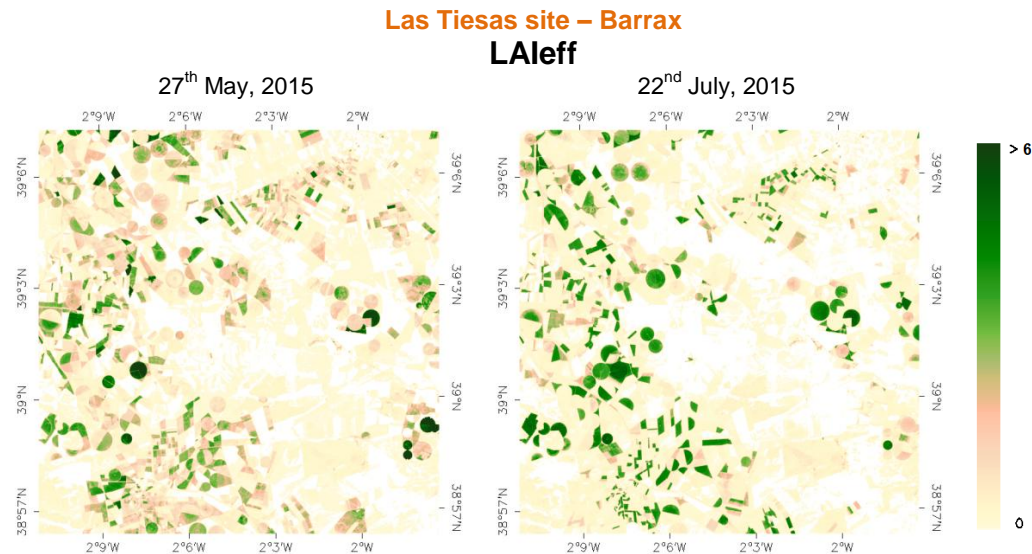


Figure 30: Ground-based LAleff maps (20x20 km²) retrieved on *Las Tiesas site – Barrax (Spain)* 2015. Left: First field campaign (27th May). Right: Second field campaign (22nd July).

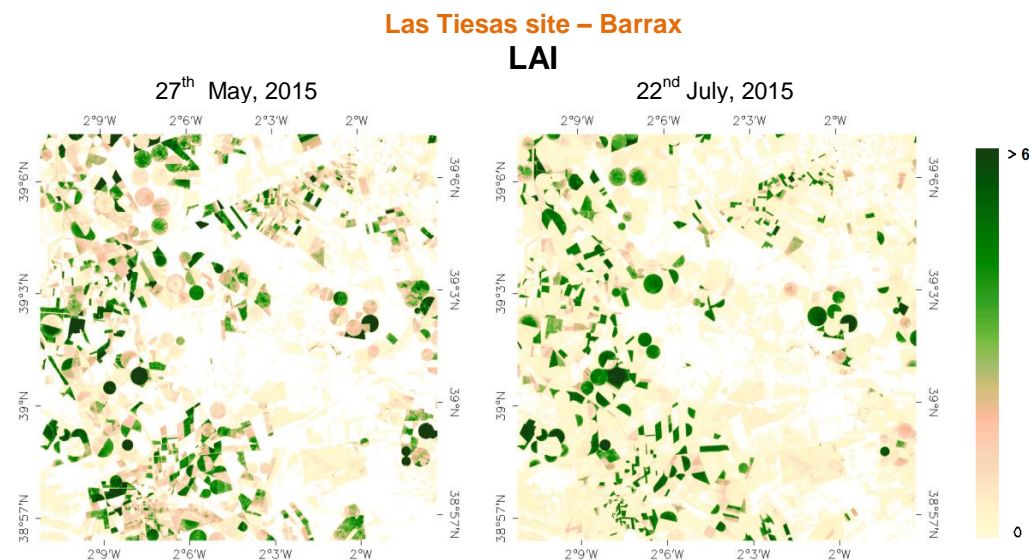


Figure 31: Ground-based LAI maps (20x20 km²) retrieved on *Las Tiesas site – Barrax (Spain)* 2015. Left: First field campaign (27th May). Right: Second field campaign (22nd July).

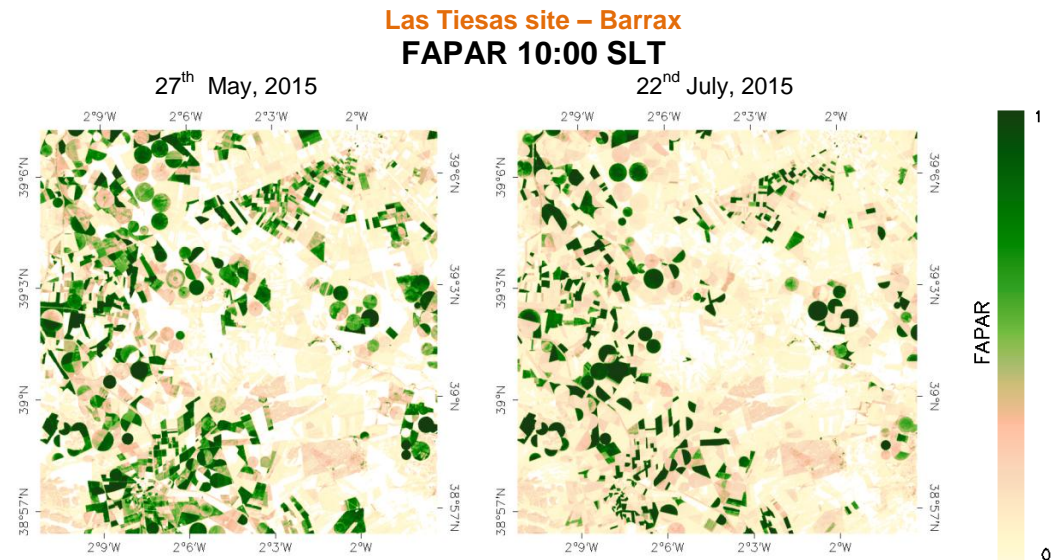


Figure 32: Ground-based of Instantaneous FAPAR at 10:00 SLT maps (20x20 km²) retrieved on *Las Tiesas site – Barrax (Spain) 2015*. Left: First field campaign (27th May). Right: Second field campaign (22nd July).

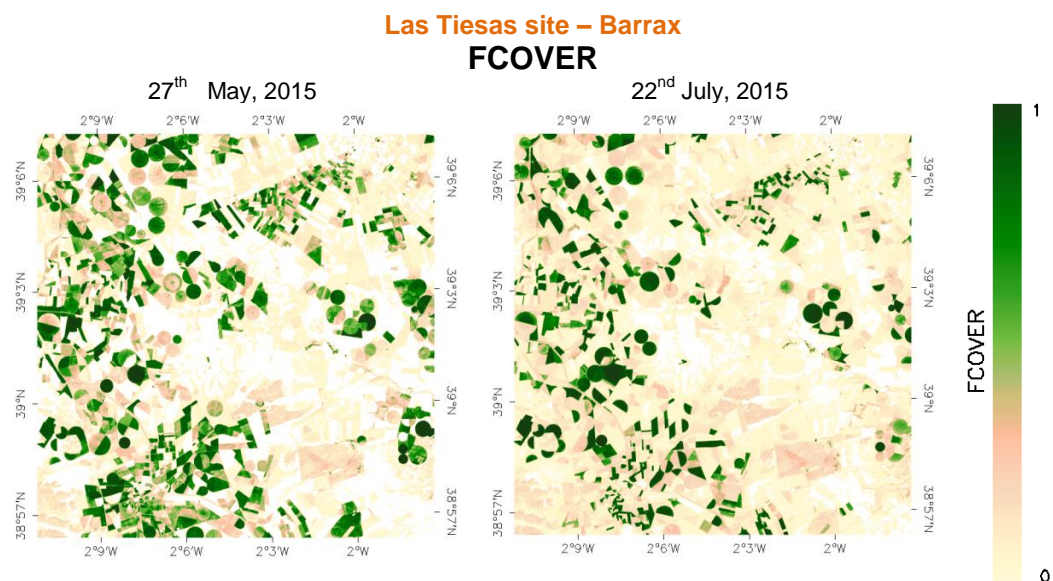


Figure 33: Ground-based FCOVER map (20x20 km²) retrieved on *Las Tiesas site – Barrax (Spain) 2015*. Left: First field campaign (27th May). Right: Second field campaign (22nd July).

Figure 34 and Figure 35 summarize these ground-based high resolution maps over the 5x5 km² study area. These maps are provided for validation of satellite products at coarser resolutions.

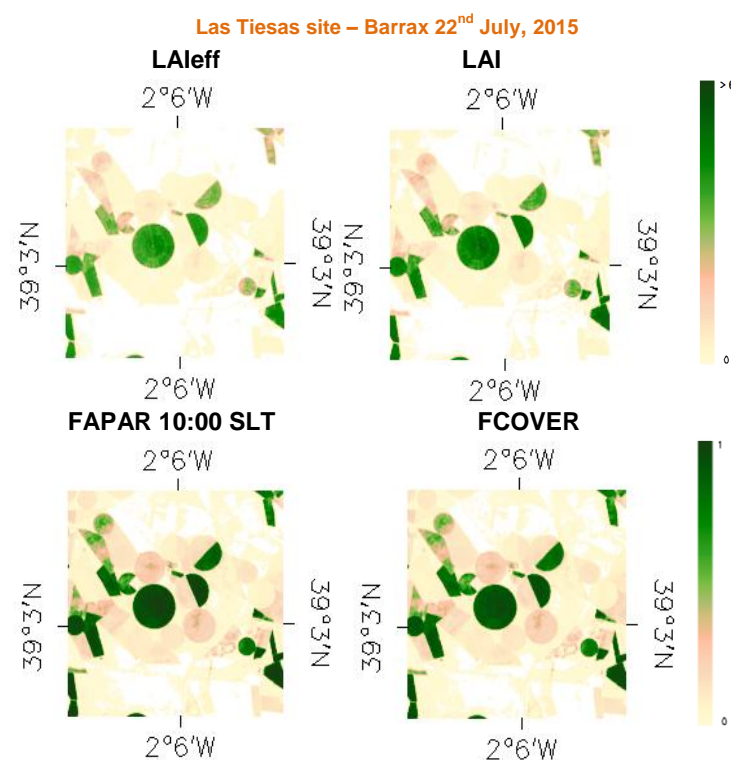
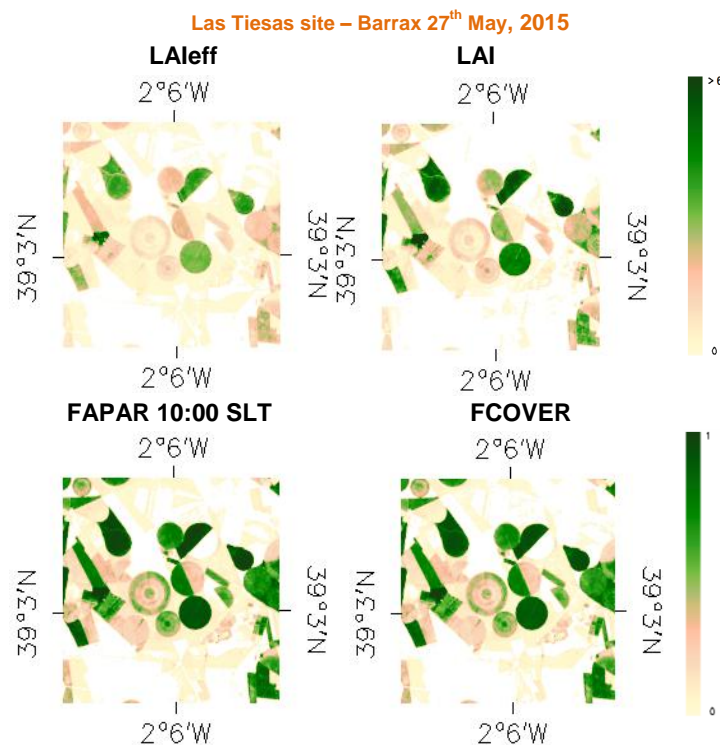


Figure 36 shows several scatters plots between biophysical variables that prove the good consistency of the 20x20 km² ground-based maps (all pixels), showing the exponential (LAI vs FAPAR) and linear (FAPAR vs FCOVER) trend observed with the ground data. Note that for the second campaign more concentration is observed over low and high values as previously reported for the ground data (see 4.3.2), mainly due to harvested and senescent fields for low values and for higher values because of corn, alfalfa and sunflower crops were at their maximum values.

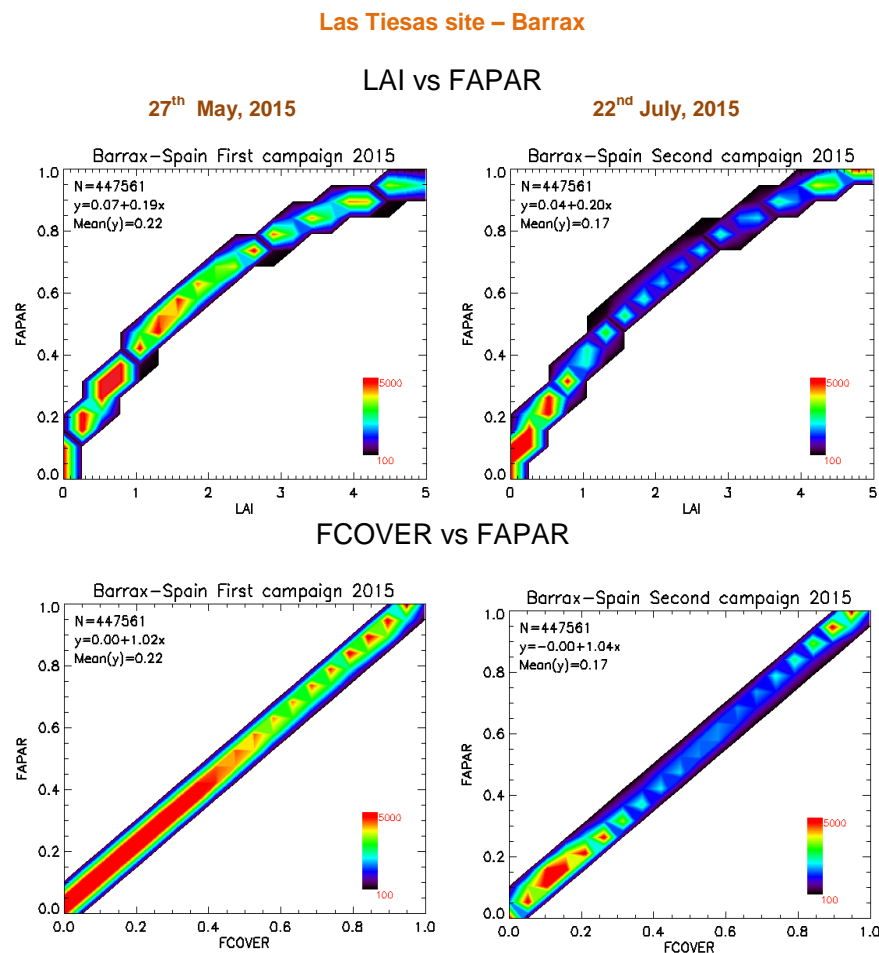


Figure 36: Scatter plots to LAI vs FAPAR and FAPAR vs FCOVER for the two campaigns over Las Tiesas site – Barrax (Spain) 2015. Left: First field campaign (27th May). Right: Second field campaign (22nd July).

6.3.1. Mean Values

Mean values of a 3x3 km² area centred in the test site are provided for the validation of 1 km satellite products in agreement with the CEOS OLIVE direct dataset (Table 6). For the validation of coarser resolutions product (e.g. MSG products) a larger area should be considered. For this reason, empirical maps are provided at 5x5 km², and 20x20 km².

Table 6: Mean values and standard deviation (STD) of the HR biophysical maps for the selected 3 x 3 km² areas at Las Tiesas site – Barrax (Spain) 2015.

Barrax Landsat-8 3x3 km ²	LATITUDE				LONGITUDE			
	39.054371				-2.100677			
	Mean Values				STDV Values			
	LAleff	LAI	FAPAR	FCOVER	LAleff	LAI	FAPAR	FCOVER
27 th May, 2015	0.74	1.01	0.29	0.27	1.03	1.52	0.31	0.30
22 nd July, 2015	0.70	0.83	0.23	0.22	1.19	1.40	0.30	0.29

Table 7 describes the content of the geo-biophysical maps in the “BIO_YYYYMMDD_LANDSAT8_Barrax ETF_20x20” files.

Nomenclature: BIO_YYYYMMDD_SENSOR_Site ETF_Area

where:

BIO stands for Biophysical (LAleff, LAI, FAPAR and FCOVER)

SENSOR = LANDSAT8

YYYYMMDD = Campaign date

Site = Barrax

ETF stands for Empirical Transfer Function

Area = window size 20x20 and 5x5

Table 7: Content of the dataset.

Parameter	Dataset name	Range	Variable Type	Scale Factor	No Value
LAI effective	LAleff	[0, 7]	Integer	1000	-1
LAI	LAI	[0, 7]	Integer	1000	-1
FAPAR 10:00 SLT	FAPAR	[0, 1]	Integer	10000	-1
Fraction of Vegetation Cover	FCOVER	[0, 1]	Integer	10000	-1
Quality Flag	QFlag	0,1,2 (*)	Integer	N/A	-1

(*) 0 means extrapolated value (low confidence), 1 strict interpolator (best confidence), 2 large interpolator (medium confidence).

7. CONCLUSIONS

The FP7 ImagineS project continues the innovation and development activities to support the operations of the Copernicus Global Land service. One of the ImagineS demonstration sites is the *Las Tiesas – Barrax* experimental site situated within La Mancha, a plateau 700 m above sea level. The test site is located in the west of province of Albacete, Spain. The area is characterized by a flat morphology with large and uniform land units.

This report firstly presents the ground data collected during two field campaigns on 27th of May and 22nd of July, 2015. The dataset includes 31 and 37 elementary sampling units where digital hemispherical photographs, were taken and processed with the CAN-EYE software to provide LAI, LAI_{eff}, FAPAR and FCOVER values. Additional measurements were collected with LAI2200 and LP80 devices over several ESUs. Several measures obtained during the field experiment have been used to control our maps on non vegetated areas or non photosynthetically active elements (senescent crops). Clumping index has set to 0.95 for very homogeneous canopies (i.e. alfalfa and papaver) to avoid overestimation of actual LAI.

Secondly, high resolution ground-based maps of the biophysical variables have been produced over the site. Ground-based maps have been derived using high resolution imagery (Landsat-8 TOC Reflectance) according to the CEOS LPV recommendations for validation of low resolution satellite sensors. Transfer functions have been derived by multiple robust regressions between ESUs reflectance and the several biophysical variables. Because the scene presents many senescent and harvested fields, we have selected the NDVI as input for the transfer function (exponential relationship with LAI_{eff} and LAI, and linear relationship with FAPAR and FCOVER). NDVI assures good consistency of the maps over the whole area. The RMSE values for the several transfer function estimates are 0.33 and 0.2 for LAI_{eff}, 0.36 and 0.15 for LAI, 0.09 and 0.03 for instantaneous FAPAR at 10:00 SLT and finally 0.13 and 0.05 for FCOVER, for the two field campaigns respectively.

The quality flag map based on the convex-hull analysis shows quite good quality (80% at 5x5 km² and 70% at 20x20 km²).

The biophysical variable maps are available in geographic (UTM 30 North projection WGS-84) coordinates at 30 m resolution. Mean values and standard deviation for LAI_{eff}, LAI, FCOVER and FAPAR were computed over an area of 3x3 km² for validation of low and medium resolution satellite products.

8. ACKNOWLEDGEMENTS

This work is supported by the FP7 IMAGINES project under Grant Agreement N°311766. Landsat-8 HR imagery is provided through the USGS Global Visualization service. This work is done in collaboration with the consortium implementing the Global Component of the Copernicus Land Service.

Thanks to the ITAP for the support and the organization of the field campaign, and the facilities which allow us to properly characterize the site.

9. REFERENCES

Baret, F., de Solan, B., Lopez-Lozano, R., Ma, K. and Weiss, M. (2010) GAI estimates of row crops from downward looking digital photos taken perpendicular to rows at 57.5° zenith angle: theoretical considerations based on 3D architecture models and application to wheat crops. *Agricultural and Forest Meteorology*. 150, 1393-1401.

Baret, F and Fernandes, R. (2012). Validation Concept. VALSE2-PR-014-INRA, 42 pp.

Berguer, M. M. Rast, P. Wursteisen, E. Attema, J. Moreno, et al. (2001). The DAISEX campaigns in support of a future land-surface-processes mission. *Esa bulletin, Bulletin ASE*. European Space Agency, n°105: 101-111, February 2001.

Calera, A., A.M. Jochum, A. Cuesta, A. Montoro and P. López Fuster (2005). Irrigation management from space: Towards user-friendly products. *Irrig. Drain. Systems*, 19, 337-353.

Camacho, F., Cernicharo, J., Lacaze, R., Baret, F., and Weiss, M. (2013). GEOV1: LAI, FAPAR Essential Climate Variables and FCOVER global time series capitalizing over existing products. Part 2: Validation and intercomparison with reference products. *Remote Sensing of Environment*, 137: 310-329.

Decagon Devices, Inc. (2014). AccuPAR PAR/LAI Ceptometer. Model LP80 manual. <http://www.decagon.com>

Demarez, V., Duthoit, S., Baret, F., Weiss, M. and Dedieu, G. (2008). Estimation of leaf area and clumping indexes of crops with hemispherical photographs. *Agricultural and Forest Meteorology*. 148, 644-655.

Fernandes, R., Plummer, S., Nightingale, J., et al. (2014). Global Leaf Area Index Product Validation Good Practices. CEOS Working Group on Calibration and Validation - Land Product Validation Sub-Group. *Version 2.0: Public version made available on LPV website*.

Latorre, C., Camacho, F., de la Cruz, F, Atienzar, F. (2015). "Vegetation Field Data and Production of Ground-Based Maps: Las Tiesas - Barrax site. Albacete, Spain. 29th -30th May 2014" report. (Available at ImagineS website: <http://fp7-imagines.eu/pages/documents.php>).

Latorre, C., Camacho, F., Pérez, M., Beget M.E. and Di Bella, C. (2014). "Vegetation Field Data and Production of Ground-Based Maps: 25 de Mayo site. La Pampa, Argentina" report. 18 -20 (Available at ImagineS website: <http://fp7-imagines.eu/pages/documents.php>).

LI-COR Inc., Lincoln, Nebraska, (2013). [http://envsupport.licor.com/docs/LAI-2200C Instruction Manual.pdf](http://envsupport.licor.com/docs/LAI-2200C%20Instruction%20Manual.pdf)

Martínez, B., García-Haro, F. J., & Camacho, F. (2009). Derivation of high-resolution leaf area index maps in support of validation activities: Application to the cropland Barrax site. *Agricultural and Forest Meteorology*, 149, 130–145.

Miller, J.B. (1967). A formula for average foliage density. *Aust. J. Bot.*, 15:141-144

Morisette, J. T., Baret, F., Privette, J. L., Myneni, R. B., Nickeson, J. E., Garrigues, S., et al. (2006). Validation of global moderate-resolution LAI products: A framework proposed within the CEOS land product validation subgroup. *IEEE Transactions on Geoscience and Remote Sensing*, 44, 1804–1817.

Weiss, M., Baret, F., Smith, G.J., Jonckheere, I. and Coppin, P., (2004). Review of methods for in situ leaf area index (LAI) determination. Part II. Estimation of LAI, errors and sampling. *Agricultural and Forest Meteorology*. 121, 37–53.

Weiss M. and Baret F. (2010). CAN-EYE V6.1 User Manual

Welles, J.M. and Norman, J.M., 1991. Instrument for indirect measurement of canopy architecture. *Agronomy J.*, 83(5): 818-825.

10. ANNEX I: DESCRIPTION OF ESUS

Table 8: Total of ESUs collected during first campaign on 27th May, 2015 over Las Tiesas – Barrax (Spain). Cardinality of fields, plot label, cardinality of ESUs, label, latitude, longitude, land cover type and date.

Plot #	Plot Label	ESU #	ESU Label	Northing Coord	Easting Coord	Instrumentation	Land Cover	Date (dd/mm/yyyy)				
1	C	1	Ca	39.06013	-2.09718	DHP	Corn	26/05/2015				
		2	Cb	39.05943	-2.09666	DHP						
		3	Cb	39.059	-2.09608	DHP						
		4	Cd	39.05976	-2.09553	DHP						
		5	Ce	39.05984	-2.09608	DHP						
2	R	6	Ra	39.05396	-2.07932	LAI-2200	Rape					
		7	Rb	39.05422	-2.07933	LAI-2200						
		8	Rc	39.05444	-2.07963	LAI-2200						
3	P1	9	P1a	39.05251	-2.07627	DHP	Pappaver					
						LAI-2200						
		10	P1b	39.0533	-2.07541	DHP						
						LAI-2200						
		11	P1c	39.05331	-2.0746	DHP						
						LAI-2200						
12	P1d	39.05286	-2.07372	DHP								
				13	P1e	39.0518	-2.07499	DHP				
4	G1	14	G1a					39.04871	-2.0704	DHP	Garlic	
		15	G1b	39.04837	-2.0708	DHP						
		16	G1c	39.0491	-2.07098	DHP						
5	G2	17	G2a	39.0561	-2.08627	DHP						
		18	G2b	39.05663	-2.08726	DHP						
		19	G2c	39.05696	-2.08795	DHP						
6	W1	20	W1a	39.04902	-2.0995	LAI-2200	Wheat	27/05/2015				
						DHP						
		21	W1b	39.04848	-2.09916	LAI-2200						
						DHP						
22	W1C	39.04807	-2.09924	DHP								
				7	P2	23	P2a	39.04922	-2.09793	LAI-2200	Pappaver	
										DHP		
						24	P2b	39.04909	-2.09762	DHP		
LAI-2200												
25	P2bc	39.04904	-2.09721	DHP								
				8	A	26	Aa	39.0548	-2.10173	LAI-2200	Alfalfa	
										DHP		
						27	Ab	39.05519	-2.10189	LAI-2200		
DHP												
28	Ab	39.05571	-2.10212	DHP								
				9	B1	29	B1a	39.05441	-2.10623	LAI-2200	Barley	
										DHP		
						30	B1c	39.05529	-2.09965	DHP		
31	B1d	39.055111	-2.099031							DHP		

Table 9: Total of ESUs collected during first campaign on 22nd July, 2015 over Las Tiesas – Barrax (Spain). Cardinality of fields, plot label, cardinality of ESUs, label, latitude, longitude, land cover type and date.

Plot #	Plot Label	ESU #	ESU Label	Northing Coord	Easting Coord	Instrumentation	Land Cover	Start Date (dd/mm/yyyy)
1	C1	1	C1a	39.05210	-2.0771	DHP	Corn	22/07/2015
						LAI-2200		
		2	C1b	39.05218	-2.07724	DHP		
		3	C1c	39.05193	-2.07728	LAI-2200		
		4	C1d	39.05196	-2.07759	DHP		
		5	C1e	39.05188	-2.07758	DHP		
2	C2	7	C2a	39.051768	-2.07661	LAI-2200		
						DHP		
						LAI-2200		
		8	C2b	39.05119	-2.07696	LAI-2200		
9	C2c	39.05153	-2.07666	LP80				
1	C1	10	C1g	39.05141	-2.07753	LP80		
3	H1	11	H1a	39.05252	-2.07632	DHP	Pappaver Harvested	
4	H2	12	H2a	39.05299	-2.0802	DHP	Barley Harvested	
5	H3	13	H3a	39.05464	-2.07941	DHP	Rape Harvested	
6	H4	14	H4a	39.06779	-2.08807	DHP	Wheat Harvested	
7	SF1	15	SF1a	39.06572	-2.08877	DHP	Sunflower	
						LP80		
		16	SF1b	39.06556	-2.08901	DHP		
		17	SF1c	39.06536	-2.08931	DHP		
		18	SF1d	39.06519	-2.08925	DHP		
						LAI-2200		
		19	SF1e	39.06532	-2.08907	LP80		
						DHP		
20	SF1f	39.06535	-2.0888	DHP				
				LAI-2200				
8	C3	21	SF1g	39.06549	-2.08864	LP80		
		22	C3a	39.06013	-2.09718	LP80	Corn	
23	C3b	39.05984	-2.09608	LAI-2200				
9	H5	24	H5a	39.04543	-2.09681	DHP	Barley Harvested	
10	H6	25	H6a	39.04549	-2.09794	DHP		
11	H7	26	H7a	39.043106	-2.096983	DHP		
12	H8	27	H8a	39.042564	-2.101	DHP		
13	H9	28	H9a	39.042108	-2.100961	DHP	Bare Soil	
14	H10	29	H10a	39.055111	-2.099031	DHP	Barley Harvested	
15	A1	30	A1a	39.05148	-2.10286	DHP	Alfalfa	
		31	A1b	39.05175	-2.10305	DHP		
		32	A1c	39.05221	-2.10264	DHP		
		33	A1d	39.05239	-2.10218	DHP		
16	H11	34	H11a	39.04904	-2.09721	DHP	Pappaver Harvested	
17	SF2	35	SF2a	39.059546	-2.106993	DHP	Sunflower	
		36	SF2b	39.060038	-2.107103	DHP		
		37	SF2c	39.059452	-2.10689	DHP		